O'Connor, L. K., Jenkyns, H. C., Robinson, S. A., Remmelzwaal, S. R. C., Batenburg, S. J., Parkinson, I. J., & Gale, A. S. (2020). A re-evaluation of the Plenus Cold Event, and the links between CO2, temperature, and seawater chemistry during OAE 2. *Paleoceanography and Paleoclimatology*, *35*(4), [e2019PA003631]. https://doi.org/10.1029/2019PA003631

A re-evaluation of the Plenus Cold Event, and the links between CO_2, temperature, and seawater chemistry during OAE 2

Lauren K. O'Connor[1]*, Hugh C. Jenkyns[1], Stuart A. Robinson[1], Serginio R.C. Remmelzwaal[2], Sietske J. Batenburg[1], Ian J. Parkinson[2], & Andy S. Gale[3]**

[1]Department of Earth Sciences, University of Oxford, UK. [2]School of Earth Sciences, University of Bristol. [3]School of Earth & Environmental Sciences, University of Portsmouth

*Now at Department of Geosciences, University of Arizona, USA.

**Now at Univ Rennes, CNRS, Géosciences Rennes, France.

Corresponding author: Lauren O'Connor (lko@arizona.edu)

Key Points:

- This study is the first to review mechanistic interactions, and temporal leads and lags, between temperature, seawater chemistry, and CO_2 within the Plenus interval
- The negative carbon-isotope excursion during the Plenus interval was a global event driven by a CO_2 increase, and appears decoupled from cooling and circulation changes
- Cooling was not globally synchronous; local climatic & environmental responses to the CO_2 change are more complex than previously understood

Abstract

The greenhouse world of the mid-Cretaceous (~94 Ma) was punctuated by an episode of abrupt climatic upheaval: Oceanic Anoxic Event 2 (OAE 2). High-resolution climate records reveal considerable changes in temperature, carbon cycling, and ocean chemistry during this climatic perturbation. In particular, an interval of cooling has been detected in the English Chalk on the basis of an invasive boreal fauna and bulk oxygen-isotope excursions registered during the early stages of OAE 2—a phenomenon known as the Plenus Cold Event (PCE), which has tentatively been correlated with climatic shifts worldwide.

Here we present new high-resolution neodymium-, carbon-, and oxygen-isotope data, as well as elemental chromium concentrations and cerium anomalies, from the English Chalk exposed at Dover, UK, which we evaluate in the context of >400 records from across the globe. A negative carbon-isotope excursion that correlates with the original 'PCE' is consistently expressed worldwide, and CO_2 proxy records, where available, indicate a rise and subsequent fall in CO_2 over the Plenus interval. However, variability in the timing and expression of cooling at different sites suggests that, although sea-surface paleo-temperatures may reflect a response to global CO_2 change, local processes likely played a dominant role at many sites. Variability in the timing and expression of changes in water-mass character, and problems in determining the driver of observed proxy changes, suggest that no single simple mechanism can link the carbon cycle to oceanography during the Plenus interval and other factors including upwelling and circulation patterns were locally important. As such, it is proposed that the Plenus carbon-isotope event is a more reliable stratigraphic marker to identify the Plenus interval, rather than any climatic shifts that may have been overprinted by local effects.

1 Introduction to Oceanic Anoxic Event 2 and the Plenus Cold Event

At a global scale, the latest Cenomanian–earliest Turonian interval was characterized by the most significant environmental perturbation of the Late Cretaceous: Oceanic Anoxic Event 2 (OAE 2; Schlanger & Jenkyns, 1976; Arthur et al., 1990; Jenkyns, 2010). OAE 2 was an interval of extreme greenhouse conditions, with high temperatures and high atmospheric pCO_2 (Arthur et al., 1988; Jenkyns et al., 1994; Kuypers et al., 1999; Jarvis et al., 2011; O'Brien et al., 2017). The leading hypothesis for the initiation of the OAE invokes the submarine emplacement of large igneous provinces releasing vast quantities of CO_2 into the ocean and atmosphere, leading to an intensified greenhouse climate that caused an accelerated hydrological cycle and enhanced nutrient flux to the oceans (e.g. Jenkyns, 2003). Volcanism and/or other types of basalt–seawater interaction may also have supplied biologically significant metals directly into seawater (Orth et al., 1993; Snow et al., 2005; Turgeon & Creaser 2008; Du Vivier et al., 2014; Jenkyns et al., 2017). Nutrient input is credited with enhancing organic productivity on a global scale, increasing the carbon flux to the sea floor to form the characteristic black-shale record and a distinctive positive $\delta^{13}C$ excursion—together constituting the hallmark of the OAE—as well as progressively leading to significant regional deoxygenation in many parts of the world ocean, particularly the North Atlantic (e.g. Pearce et al., 2009; Jenkyns, 2010). Bottom-water anoxia and hypoxia possibly affected 40–50% of the global ocean, but with euxinic (sulphidic) bottom waters affecting a much smaller percentage (Monteiro et al., 2012; Owens et al., 2013; Dickson et al., 2016, 2017; Ostrander et al., 2017).

Accelerated burial rates of planktonic organic matter, whose biosynthesis led to preferred incorporation of the lighter ^{12}C isotope, resulted in a marked positive carbon-isotope excursion recorded in different sedimentary archives around the world (e.g. Scholle & Arthur 1980;

Schlanger et al., 1987; Jenkyns et al., 1994; Tsikos et al., 2004; Bowman & Bralower 2005; Voigt et al., 2006; Jarvis et al., 2011; Wendler, 2013). The canonical model suggests that, eventually, increased rates of organic-carbon burial would have caused a drawdown of atmospheric CO_2, ultimately triggering global cooling that led to a weakening of the factors promoting carbon burial (Arthur et al., 1988; Jenkyns et al., 1994; Kuypers et al., 1999; Sinninghe Damsté et al., 2010; van Bentum et al., 2012; Gale et al., 2019).

Lithium- and calcium-isotope records suggest that, in addition to organic-carbon burial, enhanced silicate weathering in both subaerial (under conditions of an accelerated hydrological cycle) and submarine environments during the OAE may have aided in the drawdown of CO_2 and the termination of the OAE (Blättler et al., 2011; van Bentum et al., 2012; Pogge von Strandmann et al., 2013; Jenkyns et al., 2017; Jenkyns 2018). However, it has recently been argued that the persistence of high temperatures globally throughout the latter stages of OAE 2 and into the early Turonian suggests that CO_2 did not decline, and that some other mechanism was responsible for the termination of the event, rather than a cessation of climatic factors favourable for 'black shale' formation (Robinson et al., 2019).

While the sedimentary expression of the OAE 2 interval varies worldwide, the carbon-isotope evolution of OAE 2 is broadly similar in all investigated sites across the world where the stratigraphic record is tolerably complete (Figure 1): first build-up, trough, second build-up, plateau with spikes, followed by decay towards background (Paul et al., 1999; Tsikos et al., 2004; Wendler 2013).

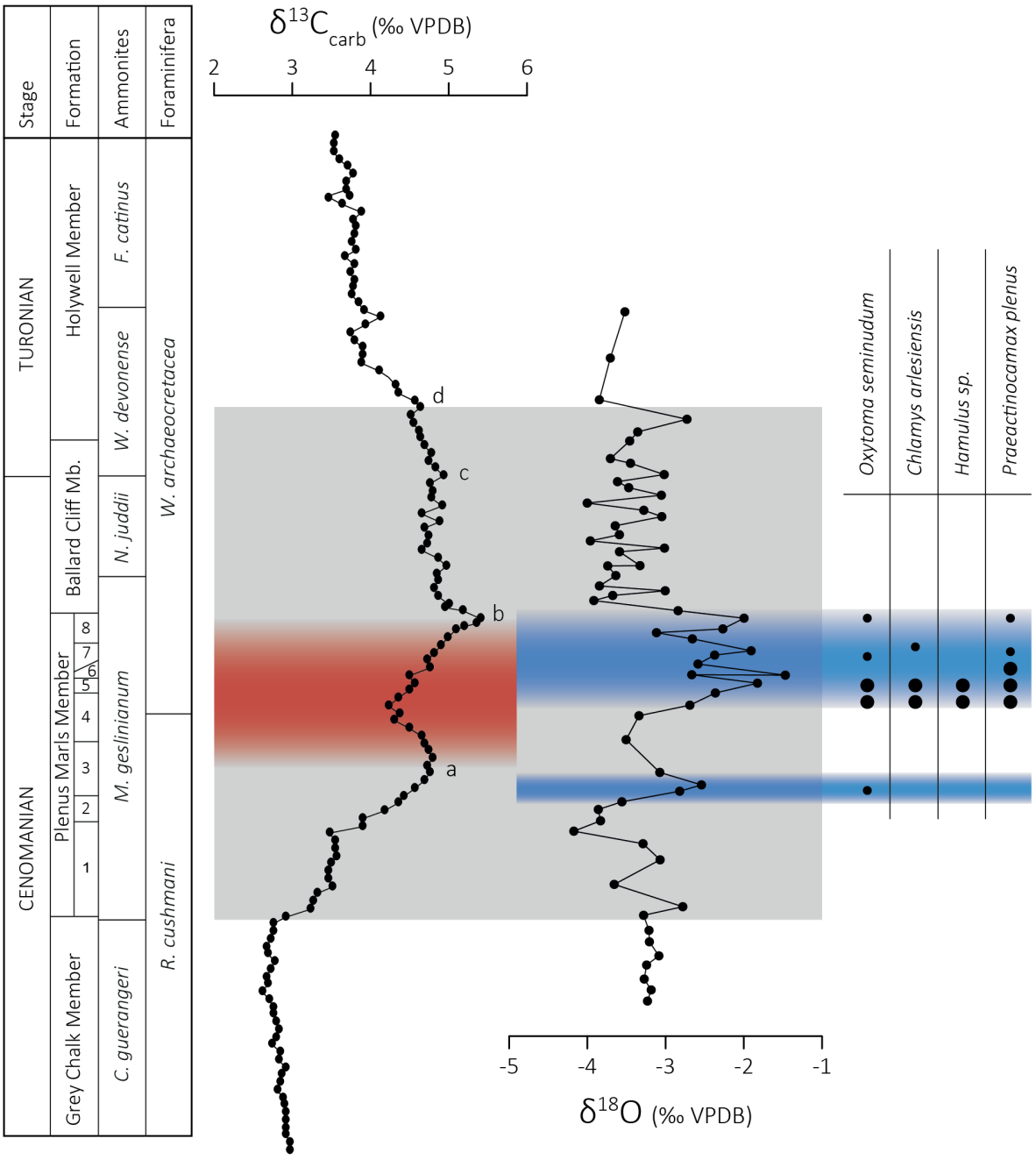

Figure 1. The composite 'type-section' recording OAE 2 and the Plenus Cold Event from the English Chalk, using $\delta^{13}C_{carb}$ from Eastbourne (Tsikos et al., 2004), and bulk $\delta^{18}O$ and boreal fauna from Dover (Lamolda et al., 1994; Gale and Christensen, 1996), correlated using the beds of the Plenus Marl Member (for details see Jarvis et al., 2006). Points 'a–d' show globally

88 consistent positions on the $\delta^{13}C$ curve (Jarvis et al., 2006). The gray box shows the interval of
89 OAE 2 (Jenkyns et al., 2017) extending from the uppermost Cenomanian to the lowermost
90 Turonian. The red bar indicates the Plenus carbon-isotope excursion, as defined in this study.
91 The blue bars indicate cooling, with the upper bar defined in this study as the PCE *sensu stricto*
92 (Gale and Christensen, 1996).

93

94 In the early stages of OAE 2, between peaks 'a' and 'b' (Figure 1), a brief (~40 kyr; Jarvis
95 et al., 2011) interval of cooling occurred that was first recognized in the chalk of the Anglo-Paris
96 Basin by the southerly incursion of boreal fauna (notably the belemnite *Praeactinocamax plenus*)
97 into the paleo-European mid-latitudes (Jefferies 1962, 1963). This interval was later discovered
98 to be coeval with a positive oxygen-isotope excursion, and it was found that the spread of Boreal
99 fauna extended southwards into the Tethys (southern France: Gale & Christensen 1996). This
100 period of cooling was termed the 'Plenus Cold Event' (PCE) after the Plenus Marls, a relatively
101 clay-rich interval in the English Chalk where the fall in temperature is registered (Figure 1;
102 Jenkyns et al., 2017). Cooling during OAE 2 has been identified from a number of SST proxies
103 from marine sections across the Northern Hemisphere (e.g. Forster et al., 2007; Sinninghe
104 Damsté et al., 2010; Jarvis et al., 2011; Desmares et al., 2016; van Helmond et al., 2016; Gale et
105 al., 2019), suggesting that the entire North Atlantic Ocean and its surrounding epicontinental seas
106 were affected. Broadly synchronous with the PCE, a period of extensive bottom-water re-
107 oxygenation occurred throughout the Western Interior Seaway of North America and the North
108 Atlantic (Eicher and Worstell, 1970; Eicher & Diner, 1985; Leckie, 1985; Keller and Pardo,
109 2004; Forster et al., 2007; Friedrich et al., 2006; Keller et al., 2008; Eldrett et al., 2014; Zhou et
110 al., 2015). The strata affected by re-oxygenation have been referred to as pertaining to the

111 'Benthic Oxic Zone', although this event is typically equated with the Plenus Cold Event (e.g.
112 Eldrett et al., 2014; van Helmond et al., 2016; Jenkyns et al., 2017), suggesting a global forcing
113 mechanism for both climatic and redox changes.

114 Many authors have attributed the PCE to a decline in atmospheric pCO_2 (e.g. Barclay et al.,
115 2010; Sinninghe Damsté et al., 2010; Jarvis et al., 2011; Gale et al., 2019), suggesting that the
116 transient negative $\delta^{13}C$ excursion signifies reduced global burial of organic carbon under more
117 oxygenated conditions, recorded at sites around the world (Erbacher et al., 2005; Voigt et al.,
118 2008; Jarvis et al., 2011; Hasegawa et al., 2013). Estimates of the magnitude of the atmospheric
119 pCO_2 decrease during OAE 2 range from 20–25% (Freeman & Hayes 1992; Jarvis et al., 2011)
120 to 40–80% (Kuypers et al., 1999). Ongoing volcanism and/or basalt–seawater interaction during
121 the early part of OAE 2 and the resultant input of greenhouse gases to the atmosphere is thought
122 to have counterbalanced the carbon drawdown, maintaining relatively high temperatures except
123 during the onset of the PCE, ultimately allowing the return to greenhouse conditions only when
124 the rate of carbon dioxide supply exceeded the rate of its sequestration (Jenkyns et al., 2017).
125 While a causal relationship has been postulated between carbon-cycle dynamics and cooling
126 during the Plenus interval (e.g. Kuypers et al., 1999; Forster et al., 2007; Sinninghe Damsté et
127 al., 2010; Jarvis et al., 2011), the existing records are from widespread locations and, as such,
128 explanations of the PCE are sensitive to the stratigraphic correlation between sites.
129 Understanding the timing of paleoenvironmental changes, both local and global, is therefore
130 critical for disentangling the driver of climate change during this perturbation of the carbon
131 cycle. As such, we seek here to investigate the synchroneity of environmental changes at the
132 location where the PCE was first recognized, and to contextualize these data by synthesising all

133 available records to investigate the global responses of carbon-cycling, temperature, and
134 seawater chemistry around the time of the PCE.

135

136 **2 Materials and Methods**

137 2.1 Plenus Marls, Dover

138 This study was conducted on the ~3 m thick Plenus Marls section near Shakespeare Cliff
139 (Dover, UK; Figure 1), a well-known section for the study of OAE 2 (Schlanger et al., 1987).
140 This site was located at a paleolatitude of ~42°N during the OAE (Van Hinsbergen et al., 2015),
141 within the main part of the Anglo-Paris Basin. Across the basin, the Plenus Marls generally
142 consist of a discrete unit of clay-rich chalks sandwiched between clay-poor chalks; the section at
143 Dover comprises rhythmically bedded chalks and marls, rich in planktic foraminifera,
144 nannofossils, macrofauna and clays (Jefferies 1962, 1963; Jeans et al., 1991). Jefferies (1962;
145 1963) introduced a numbering system for these beds (numbered 1–8), which has been generally
146 adopted and followed in this study. The Shakespeare Cliff exposure at Dover is one of the best
147 onshore sections for geochemical studies, as there has been relatively little diagenetic alteration
148 of the chalk (Scholle et al., 1974). Previous studies argued that, although foraminiferal $\delta^{18}O$ had
149 been lowered by burial diagenesis, the relative trends were still reliable for paleoclimatic
150 interpretation (Corfield et al., 1990; Jeans et al., 1991; Jenkyns et al., 1994; Lamolda et al.,
151 1994).

152 The Plenus Marls were deposited in an epicontinental pelagic shelf sea during a major
153 transgressive phase (Hancock 1993). During the mid-Cretaceous, this location was connected

154 with the Boreal Sea to the north, the Tethys to the south, and the North Atlantic to the west
155 (Hancock 1975; Hancock & Kauffman 1979).

156 2.2 Sampling and sample preparation

157 Samples were collected every 10 cm from above and below the erosional base of the
158 Plenus Marls up to Bed 8, with two additional samples at a 30 cm spacing from the overlying
159 chalk. Samples were oven-dried for 48 hours at 40°C to remove residual water and the edges
160 were scraped clean using a metal spatula to remove any loose rock debris or other detritus.
161 Samples were then ground to a fine powder using an agate pestle and mortar, and homogenized.

162 2.4. Stable carbon and oxygen isotopes

163 Bulk carbonate samples were oxidized to remove organic matter by means of H_2O_2 (15%,
164 pH 8) being added to each sample and allowed to react for 30 minutes, then oven-dried at 40°C.
165 Measurements were performed on a Delta V Advantage isotope mass spectrometer fitted with a
166 Gas Bench II in the Department of Earth Sciences (University of Oxford); the carbonates were
167 converted to CO_2 with 100% H_3PO_4. Three internal standards were used that have previously
168 been calibrated to international reference materials: CarreraCam, Wiley, and NOCZ (n = 2, 2, 5
169 respectively). Respective $\pm 1\sigma$ values are 0.04, 0.02, and 0.03% for $\delta^{13}C$, and 0.02, 0.07, and
170 0.02% for $\delta^{18}O$. In-house marble standard NOCZ has a long-term external repeatability of 0.07%
171 for $\delta^{13}C$ and 0.09 for $\delta^{18}O$. $\delta^{18}O$ and $\delta^{13}C$ values are expressed in per mil variations relative to
172 VPDB.

173 2.5. Neodymium isotopes

174 Nd was extracted from bulk chalk using the method of Zheng et al. (2013), followed by
175 the standard two-stage ion-exchange column separation technique (Pin & Santos Zalduegui

1997). In short, 20 ml of 10% acetic acid was added to 5 g of powdered sample, and allowed to react for 2 hours. The samples were centrifuged, after which the supernatant was pipetted off, dried down, re-dissolved in 6 M HCl and dried down again, and finally re-dissolved in 1 M HCl before column chemistry. Rare-earth elements were separated from major cations using 0.8 mL AG50W-X12 (200–400 μm) resin with 6M HNO_3 as an eluent. On a second column, Nd was separated from other REEs using 125 μl of Ln spec (20–40 μm) resin with 0.25M HCl as an eluent.

Nd isotopes ($\varepsilon_{Nd(t)}$) were analysed on an MC-ICP-MS (NuPlasma) in the Department of Earth Sciences (University of Oxford). Mass bias was corrected by using $^{146}Nd/^{144}Nd = 0.7219$ with an exponential law. Samples were measured by bracketing with the JNdi-1 Nd isotope standard, and the instrument drift was corrected by normalizing $^{143}Nd/^{144}Nd$ ratios of the bracketing JNdi-1 to a reference value of 0.512115 (Tanaka et al., 2000). Total procedural blanks yielded ≤355pg Nd, which is negligible compared to the minimum sample yield of 27 ppb Nd (sample DPM 140). The JNdi-1 standard had an external long-term reproducibility of ~0.4 ε_{Nd} (2σ), without application of a drift correction.

2.6. Chromium and rare-earth element concentrations

Approximately 0.01 g of the bulk carbonate sample was dissolved in 0.5 M acetic acid. The solutions so produced were subsequently dried down and re-dissolved in 2% HNO_3 to form a solution containing approximately 100 ppm Ca. Standard solution mixtures containing a suite of synthetic standards of 40 trace elements including chromium and the rare-earth elements (REE) and doped with 100 ppm Ca were used to produce a calibration curve. Cr, Ce, Pr, and Nd concentrations were measured on an Agilent 7500s ICP-QQQ-MS at the Open University in O_2 and He collision mode, respectively. Cerium concentrations were normalized to post-Archaean

Australian Shale (PAAS) concentrations (Taylor and McLennan, 1985). Cerium anomalies are expressed as $Ce/Ce^* = (Ce_{sample}/Ce_{PAAS})/[Pr_{sample}/Pr_{PAAS}*(Pr_{sample}/Pr_{PAAS})/(Nd_{sample}/Nd_{PAAS})]$ (Tostevin et al., 2016). Measurements are reproducible within 2% for Cr and 9% for Ce/Ce* based on replicate analyses of JDo-1 (a carbonate standard reference material).

3. Results

3.1. Stable carbon and oxygen isotopes

$\delta^{13}C_{carb}$ ranges from 2.57–5.21‰ (Figure 2), with a minor negative excursion at the level of the lower–middle part of Bed 7 in the Plenus Marls. The record shows positive shifts at Beds 2 (peak 'a') and 8 (peak 'b'), though the trough between Beds 4 and 8 is not well expressed. The excursion documented here corresponds to excursions seen in other $\delta^{13}C_{carb}$ records from Dover and Eastbourne (Jarvis et al., 1988; Jeans et al., 1991; Lamolda et al., 1994; Gale & Christensen 1996; Paul et al., 1999; Tsikos et al., 2004; Gale et al., 2005; Voigt et al., 2006; Pearce et al., 2009; Zheng et al., 2016).

The new Dover record shows $\delta^{18}O$ varying between -4.14 and -1.98‰ with a positive shift at Bed 2 and a more significant positive excursion across Beds 6–8 characterized by a double peak indicating two phases of relatively greater $\delta^{18}O$ values, which coincide with the main marls (Figure 2).

3.2. Neodymium isotopes

Thirty-five samples had sufficient neodymium concentrations to allow measurement of Nd isotopes, which ranged from -10.3 to -8.4 ε units (Figure 2). This record shows a well-resolved 1.5 ε unit positive excursion, synchronous with the main cooling event, suggesting a change in water-mass chemistry in the Chalk Sea across southern England in the latest Cenomanian. The timing and magnitude of the positive excursion correlates well with the ε_{Nd} record from Eastbourne; however, the new data do not show the earlier negative excursion recorded in Beds 2–4 at Eastbourne (Zheng et al., 2013), possibly owing to the presence of hiatuses and condensed horizons in the Dover section (cf. Gale et al., 1993; Jarvis et al., 2006). In a previous study of the Plenus Marls at Eastbourne, fish debris and bulk carbonates from the same stratigraphic levels

were found to record nearly identical $\varepsilon_{Nd(t)}$ values (Zheng et al., 2013, 2016). As such, the $\varepsilon_{Nd(t)}$ record here is interpreted dominantly to reflect bottom-water values.

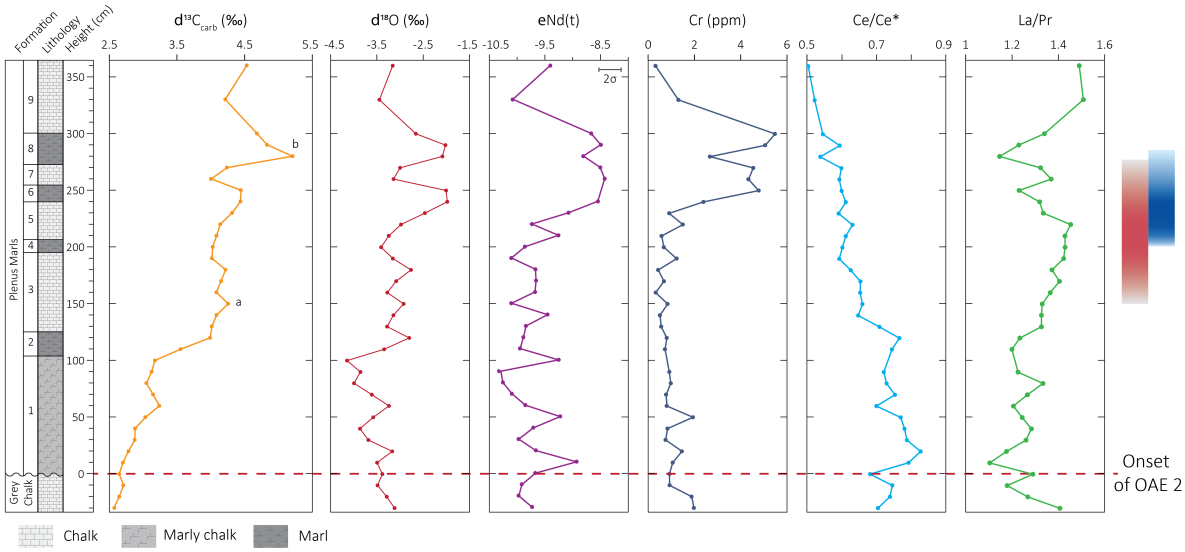

Figure 2. New geochemical data from the Plenus Marls at Dover, UK. Points 'a' and 'b' are identified on the $\delta^{13}C$ curve. With the exception of ε_{Nd}, error bars are smaller than the data points. The red dotted line indicates the onset of OAE 2; the red bar indicates the Plenus carbon-isotope excursion; the blue bar indicates the PCE *sensu stricto*.

3.3. Chromium and cerium concentrations

Chromium and REE concentrations were determined in 35 samples, with chromium concentrations ranging from 0.32–5.48 ppm, with the highest values found in Beds 6–8 of the Plenus Marls (Figure 2). Chromium concentrations peak during the uppermost Plenus interval, reflecting the pattern observed in $\delta^{18}O$. However, the response of Cr lags slightly behind the peaks in $\delta^{18}O$. Previous studies on the Plenus Marls at Eastbourne, Sussex have also identified pulses of Cr enrichment during the Plenus interval (Orth et al., 1993; Pearce et al., 2009; Jenkyns et al., 2017).

243 REE patterns yielded Ce/Ce* data with Ce anomalies between 0.5–0.85. The Ce/Ce*
244 anomalies generally decrease up-section, mirroring the generally increasing pattern of $\delta^{13}C$.
245 While Cerium anomalies are lower during the Plenus interval than prior to the event, there are no
246 observable excursions superimposed onto the decreasing trend (cf. Lu et al., 2010).
247

248 **4 Discussion of Plenus Cold Event records**

249 Because the Plenus event was first identified in the Chalk of southern England, these
250 exposures will be considered as comprising a composite type-section (Figure 1), using the
251 $\delta^{13}C_{carb}$ record of Tsikos et al. (2004) from Eastbourne and the $\delta^{18}O$ record of Lamolda et al.
252 (1994) from Dover, which also yielded the boreal fauna identified by Gale and Christensen
253 (1996). All other records will be correlated to and compared with this composite record. The
254 negative $\delta^{13}C$ excursion between peaks 'a' and 'b' is henceforth referred to as the Plenus carbon-
255 isotope excursion (P-CIE), and the interval of cooling during the 'second build-up' will be called
256 the Plenus Cold Event, *sensu stricto* (after Gale and Christensen, 1996). Using this definition,
257 and based on the age model of Kuhnt et al. (2017), the P-CIE lasted ~65 kyr, while the main
258 phase of the cooling (as seen at Eastbourne) lasted ~40 kyr.

259 4.1 Evidence for change in the carbon cycle

260 Across the globe, negative carbon-isotope excursions recording the P-CIE are registered
261 in bulk carbonate, bulk marine and terrestrial organic-matter, and compound-specific materials
262 (Figure 3). Notably, the Plenus CIE shows remarkable consistency in its timing and expression
263 across the world in terms of its relationship to, and position in, the overarching positive
264 excursion characteristic of the Cenomanian–Turonian interval. However, care must be taken
265 when interpreting these records in terms of global changes in carbon cycling as local processes

may overprint any global signal. For example, short-term local variations in $\delta^{13}C$ may reflect a direct response to transgression–regression cycles, which affect the area of shelf and marginal seas as major sinks for organic matter, or changes in oceanic ^{12}C storage in response to changing ocean circulation (Jenkyns et al., 1994; Voigt, 2000). Changes in local upwelling may also affect the $\delta^{13}C$ record, with waters coming from oxygen-minimum zones having lower seawater $\delta^{13}C$ than near-surface dissolved inorganic carbon (Berger and Vincent, 1986). As such, local oceanographic feedbacks may have produced carbon-isotope excursions partially decoupled from the isotopic composition of the global ocean–atmosphere carbon reservoir.

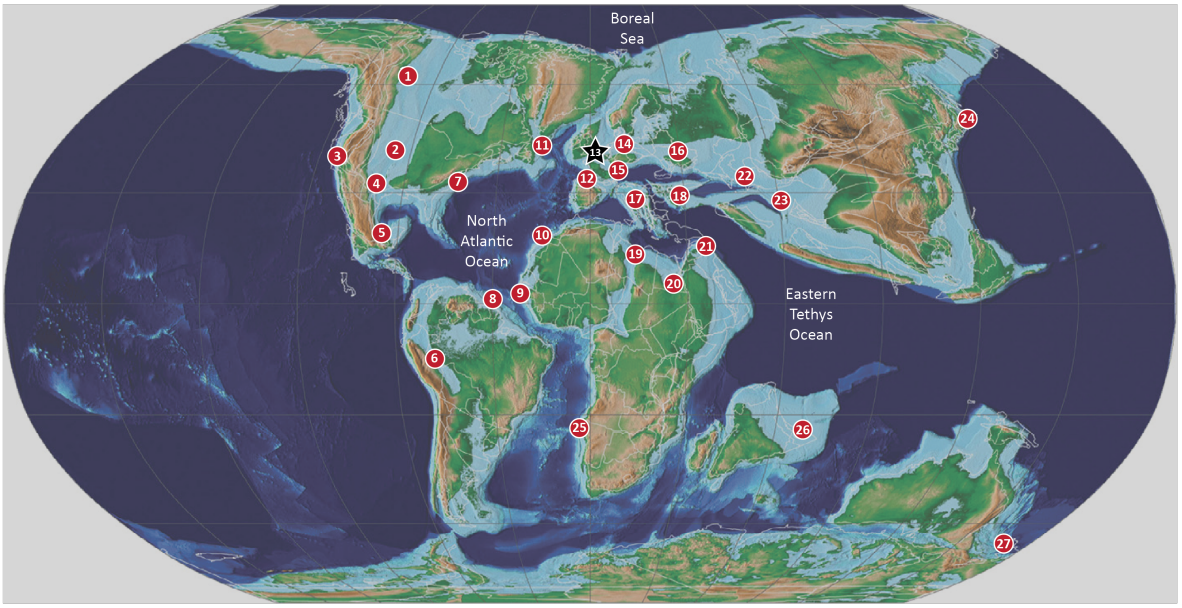

Figure 3. Global distribution of known records demonstrating the Plenus CIE (a negative $\delta^{13}C$ excursion between points 'a' and 'b' in Figure 1) or an excursion in CO_2 across the Plenus interval, as indicated by $\Delta^{13}C$, compound-specific $\delta^{13}C$, or leaf stomata. **1** Pratt's Landing (van Helmond et al., 2016); Vermillion River, Well 10-35-45-2WA (Prokoph et al., 2013). **2** Cuba, KS (Bowman & Bralower 2015); Pueblo (Barclay et al., 2010; Bowman & Bralower, 2005; Caron et al., 2006; Keller et al., 2008; Pratt et al., 1985; Sageman et al., 2006); USGS Portland-1

281 core (Eldrett et al., 2017); Aristocrat Angus core (Joo and Sageman, 2014); Hot Springs, CO
282 (Desmares et al., 2007); SH#1 core (Jones et al., 2019); generalized Western Interior Seaway
283 (Orth et al., 1993). **3** Great Valley Sequence, CA (Du Vivier et al., 2015). **4** Innes-1 core, Iona-1
284 core, Well X core (Eldrett et al., 2017). **5** Axaxacoalco, Barranca el Tigre, Barranco el Canon
285 (Elrick et al., 2009). **6** Laurichocha, Piedra Parada, Uchucchacua (Navarro-Ramirez et al., 2016,
286 2017). **7** Bass River, NJ (Bowman and Bralower, 2005; van Helmond et al., 2013). **8** ODP Site
287 1258 (Erbacher et al., 2005); ODP Site 1260 (Eldrett et al., 2017; Erbacher et al., 2005; Forster et
288 al., 2007: van Bentum et al., 2012); ODP Site 1261 (Eldrett et al., 2017; Erbacher et al., 2005). **9**
289 DSDP Site 367 (Dickson et al., 2016; Forster et al., 2007; Kuypers et al., 1999; Sinninghe
290 Damsté et al., 2008). **10** Tarfaya (Keller et al., 2008; Kolonic et al., 2005; Kuhnt et al., 2017;
291 Kuypers et al., 2002; Tsikos et al., 2004); Mpl, S57, S75 (Kolonic et al., 2005); S13 (Kuypers et
292 al., 1999; Kolonic et al., 2005). **11** ODP Site 1276 (Sinninghe Damsté et al., 2008; van Helmond
293 et al., 2014). **12** Arobes, Ganuza, Menoyo (Kaiho et al., 2014); Manilvala (Mort et al., 2007);
294 Puentedey (Barroso-Barcenilla et al., 2011). **13** Dover (this study; Jeans et al., 1991; Lamolda et
295 al., 1994); Eastbourne (Jenkyns et al., 1994; Paul et al., 1999; Tsikos et al., 2004; Gale et al.,
296 2005; Pearce et al., 2009; Zheng et al., 2013); Culver Cliff (Jarvis et al., 2001). **14** Gröbern
297 (Voigt et al., 2006); Halle (Voigt et al., 2007); Wunstorf (Voigt et al., 2008; Du Vivier et al.,
298 2014); Roter Sattel (Charbonnier et al., 2018). **15** Lambruisse (Takashima et al., 2009); Pont
299 d'Issole (Grosheny et al., 2006; Jarvis et al., 2011); les Lattes, Le Bourgeut (Grosheny et al.,
300 2017); Cassis (Heimhofer et al., 2018); Clot Chevalier (Gale et al., 2019). **16** Pecínov, Czech
301 Republic (Košťák et al., 2017). **17** Bottaccione (Kuroda et al., 2007); Furlo (Mort et al., 2007);
302 Gubbio (Jenkyns et al., 1994; Tsikos et al., 2004); Raia del Pedale (Owens et al., 2013); Monte
303 Coccovello, Monte Varchera (Parente et al., 2008). **18** Crimea (Fisher et al., 2005). **19** Jerissa

(Zaghbib-Turki & Soua 2013); Oued Mellegue (Nederbragt & Fiorentino 1999); Wadi Bahoul (Caron et al., 2006). **20** Wadi Feiran (El-Sabbagh et al., 2011). **21** Ghawr Al Mazar (Wendler et al., 2016); Wadi Karak (Farouk et al., 2017). **22** Aimaki, Khadzhalmakhi, Levashi (Gavrilov et al., 2013). **23** Taherabad (Kalanat et al., 2018). **24** Tappu (Nemoto & Hasegawa 2011); Yezo (Du Vivier et al., 2015). **25** ODP Site 530 (Forster et al., 2008). **26** Gongzha (Bomou et al., 2013); Tingri (Li et al., 2006). **27** Sawpit Gully, Mangaotane B (Hasegawa et al., 2013; Gangl et al., 2019); Mangaotane A (Hasegawa et al., 2013).

The carbon-isotope signature of bulk organic matter is especially susceptible to modification by shifts in its composition due to changes in source, preservation, and diagenetic alteration (e.g. Voigt et al., 2006). In many studies, diagenesis has been noted as potentially producing false excursions that make it difficult to determine whether the $\delta^{13}C_{org}$ records reflect paleoenvironmental change or simply local overprinting (Voigt, 2000; Voigt et al., 2006; Jarvis et al., 2006). Changing the ratio of terrestrial to marine organic matter, by either increased input or preferential preservation, will shift the $\delta^{13}C$ of the bulk material, potentially giving a false excursion unrelated to global or local carbon cycling. In several instances, bulk-organic and compound-specific $\delta^{13}C$ records from a single section show differences between these archives in the structure of the excursion through the OAE 2 interval (e.g. ODP Site 1276, Cape Verde Basin, Sinninghe Damsté et al., 2010; Figure 4), possibly owing to differences in local carbon-cycle processes, as well as changes in the relative abundance of different organic components (Tsikos et al., 2004; Kolonic et al., 2005; Sinninghe Damsté et al., 2010; Gale et al., 2019). Furthermore, differences in the pattern of the $\delta^{13}C_{carb}$ and $\delta^{13}C_{org}$ curves can also be seen within a single section, such as at Tarfaya (Tsikos et al., 2004; Kuhnt et al., 2017), which may indicate

variable fractionation between organic and inorganic carbon, local changes in carbon cycling, and/or possibly diagenetic overprints on the carbonate and/or organic fractions (Jarvis et al., 2006). However, allowing for minor differences due to the aforementioned factors, $\delta^{13}C$ curves shows a generally globally consistent evolution across the OAE and Plenus interval at most localities.

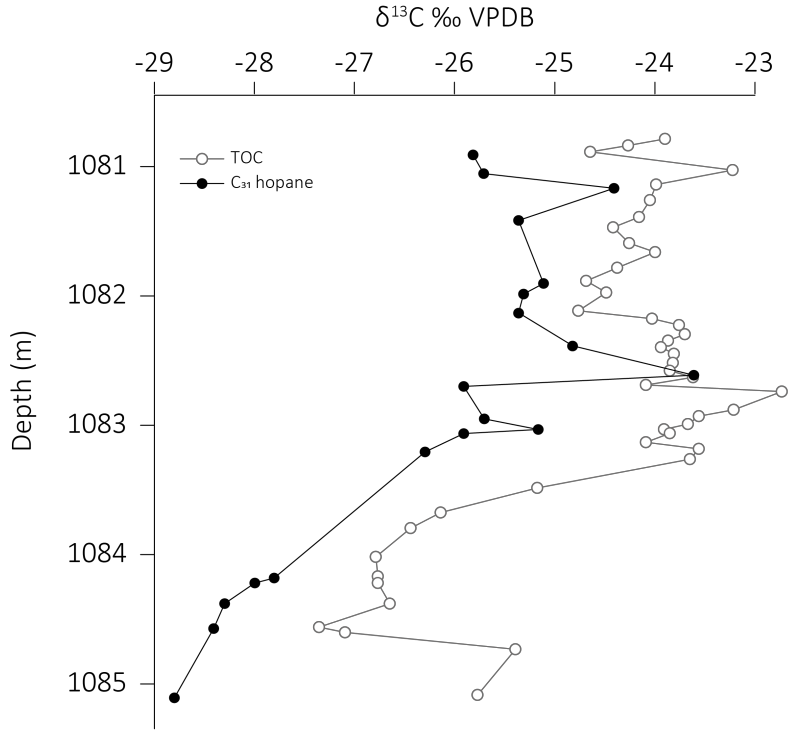

Figure 4. Comparison of $\delta^{13}C_{org}$ and $\delta^{13}C_{hopane}$ records from ODP Site 1276, Cape Verde Basin (adapted from Sinninghe Damsté et al., 2010) demonstrating a stratigraphic offset in the position of the negative excursion seen in $\delta^{13}C_{org}$ at ~1083.1 mbsf and in $\delta^{13}C_{hopane}$ at ~1082.8 mbsf.

337 4.1.1. Evidence for change in CO_2

338 Reconstructions of atmospheric CO_2 across OAE 2 are few in number (Figure 5) and, in
339 some cases, open to interpretation. A reconstruction of pCO_2, based upon values of the stomatal
340 index of fossil leaves from the margins of the Western Interior Seaway, indicates two increases
341 in pCO_2 values during the early stages of OAE 2, coincident with negative $\delta^{13}C_{org}$ excursions
342 (Barclay et al., 2010). These authors do not specify which event they think correlates with the
343 PCE, but do interpret the decreased stomatal index values as reflecting a global increase in
344 atmospheric pCO_2 in response to carbon burial. Using integrated bio- and chemostratigraphy, we
345 interpret the P-CIE as the negative $\delta^{13}C$ excursion between 25 and 50 m height (Figure 5, cf.
346 Laurin et al., 2019), consistent with the interpretation of Jarvis et al., (2011). While the stomatal
347 data are very sparse across this interval, atmospheric CO_2 appears to rise from point 'a' (Figure
348 5). Regardless of which negative excursion is interpreted to be the P-CIE, a fall in $\delta^{13}C$ correlates
349 with a rise in pCO_2. Leaf-wax $\delta^{13}C$ records from the Cenomanian–Turonian organic-rich
350 sediments from the equatorial Atlantic (Kuypers et al., 1999; Sinninghe Damsté et al., 2010) and
351 France (Heimhofer et al., 2018) suggest a rise in CO_2 from point 'a' to the trough of the P-CIE
352 and then a fall to point 'b' (Figure 5). Given the similarity in CO_2 trends indicated by these two
353 independent proxies for atmospheric CO_2, we suggest that the rise in pCO_2 from point 'a' and
354 fall across point 'b' likely reflect global changes in the atmosphere.

355 $\Delta^{13}C$ (the offset between $\delta^{13}C_{carb}$ and $\delta^{13}C_{org}$ in marine sediments) reflects the degree of
356 carbon fractionation during photosynthesis, which is pCO_2-dependent (Farquhar et al., 1989;
357 Freeman & Hayes 1992). $\Delta^{13}C$ records changes in dissolved seawater CO_2 concentration, which
358 is assumed to be in equilibrium with atmospheric CO_2, and thus can be used as a pCO_2 proxy.
359 $\Delta^{13}C$ marine records from the UK, France, Germany, and Morocco show a similar trend to the

terrestrial records from the Western Interior Seaway: namely, a rise then fall in CO_2 over the P-CIE interval (Gale et al., 2005; Voigt et al., 2006, 2007; Jarvis et al., 2011). Two $\Delta^{13}C$ records from France (Gale et al., 2019) and Iran (Kalanat et al., 2018) show different trends: both indicate an increase in pCO_2 over the P-CIE, though both show poorly resolved Plenus CIEs owing to condensation, diagenesis, or poorly resolved stratigraphy.

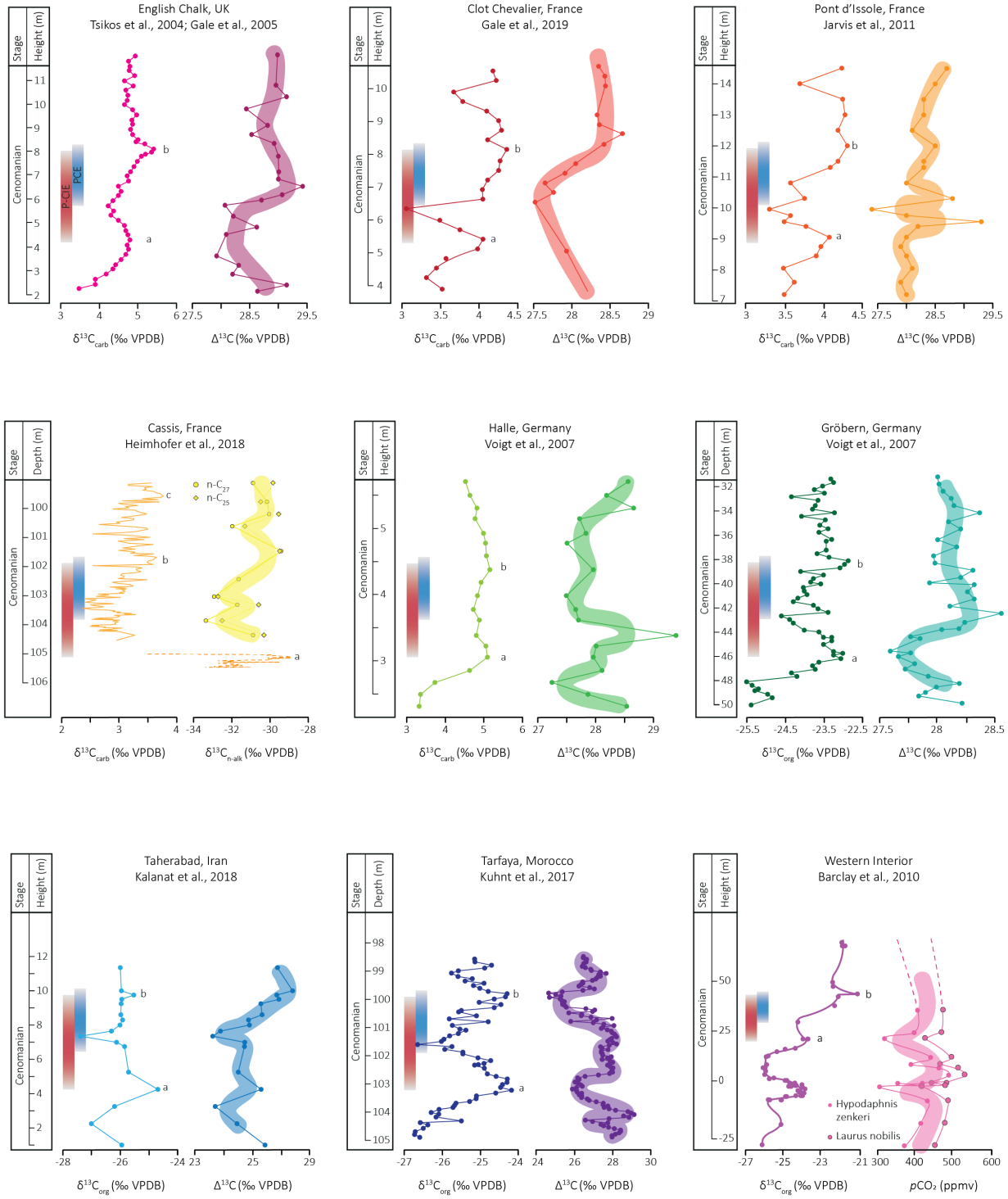
English Chalk, UK
Tsikos et al., 2004; Gale et al., 2005
Clot Chevalier, France
Gale et al., 2019
Pont d'Issole, France
Jarvis et al., 2011
Cassis, France
Heimhofer et al., 2018
Halle, Germany
Voigt et al., 2007
Gröbern, Germany
Voigt et al., 2007
Taherabad, Iran
Kalanat et al., 2018
Tarfaya, Morocco
Kuhnt et al., 2017
Western Interior
Barclay et al., 2010
Stage
Height (m)
Depth (m)
Cenomanian
P-CIE
PCE
n-C27
n-C25
Hypodaphnis zenkeri
Laurus nobilis
δ13Ccarb (‰ VPDB)
Δ13C (‰ VPDB)
δ13Cn-alk (‰ VPDB)
δ13Corg (‰ VPDB)
pCO2 (ppmv)

365

366 **Figure 5.** Records of CO_2 change across the Plenus interval. The gray boxes indicate the OAE 2
367 interval; the red boxes indicate the P-CIE; the blue boxes indicate the PCE *sensu stricto*; points
368 'a' to 'c' of the OAE are labelled. Coloured bands illustrate visual approximations of trends.

369

370 Despite their general agreement with the terrestrial proxies for pCO_2, $\Delta^{13}C$ records must
371 be treated with some caution when interpreted in the context of atmospheric CO_2 changes.
372 Changes in oceanography may have generated local variations in ocean CO_2 fluxes and
373 concentrations. For example, the incursion of a cold, oxygenated water-mass across a region
374 would have led to the remineralisation of buried organic-matter, causing a localised increase in
375 $[CO_2]$ in bottom waters and potentially, particularly in areas of upwelling, to CO_2 outgassing to
376 the atmosphere. As the total organic-carbon (TOC) content of strata varied regionally, the degree
377 of remineralization would have varied between sites, producing different CO_2 concentrations in
378 different locations. Furthermore, as CO_2 solubility is dependent on water temperature (e.g.
379 Broecker & Peng 1974), a cold water-mass would contain higher concentrations of dissolved
380 CO_2 compared with warmer waters, and this alone would have affected the local pH without
381 involving any atmospheric processes. Euxinic conditions may also affect local CO_2
382 concentrations, as the degradation of organic-matter allows phosphate to be released back to
383 bottom-waters, driving increased productivity and organic-matter deposition (Mort et al., 2007;
384 Jarvis et al., 2011). These local processes could potentially mask any signal of atmospheric pCO_2
385 change and, if not recognized, could lead to erroneous interpretations of the drivers of the PCE.

386 ### 4.2 Evidence for changing temperature

387 The Plenus Cold Event was first recognized based on the southerly migration of boreal
388 fauna coincident with two positive $\delta^{18}O$ excursions in the Chalk of Dover, UK (Jefferies et al.,
389 1962; Gale & Christensen 1996). In the Dover Chalk records, cooling is observed in Beds 2 and
390 4–8 of the Plenus Marls (Figures 1 and 2), supported by numerous other records of faunal
391 assemblages and $\delta^{18}O$ from southeast England, with some variation in the timing of the onset of
392 cooling (this study; Jefferies, 1962, 1963; Jeans et al., 1991; Lamolda et al., 1994; Paul et al.,
393 1999; Tsikos et al., 2004; Voigt et al., 2004, 2006; Gale et al., 2005). The main phase of cooling
394 in southeast England, as exemplified by the carbon-isotope record, extends from the trough of
395 the P-CIE to point 'b'.

396 The early stages of OAE 2 have been studied extensively across the Northern Hemisphere,
397 with multiple quantitative and qualitative records indicating brief cooling around the P-CIE
398 interval (Figure 6). $\delta^{18}O$ (Kuhnt et al., 2017; Kalanat et al., 2018), TEX_{86} (Forster et al., 2007;
399 Sinninghe Damsté et al., 2010), faunal assemblages (van Helmond et al., 2013, 2016; Eldrett et
400 al., 2017), and foraminiferal coiling direction (Desmares et al., 2016) show clear evidence for
401 cooling across the Tethyan margins, North Atlantic, and Western Interior Seaway. In France and
402 Germany, incursions of boreal fauna and dinocysts also indicate cooling, as supported by $\delta^{18}O$
403 and TEX_{86} records (Figure 7; Takashima et al., 2009; Voigt et al., 2006, 2007, 2008; van
404 Helmond et al., 2015). However, some bulk $\delta^{18}O$ records from hemipelagic clay-rich carbonates
405 (e.g. Pont d'Issole, Vocontian Basin, France) show no clear excursion across the PCE interval
406 (Voigt et al., 2006; Jarvis et al., 2011), even though nearby sections, a few tens of kilometres
407 away, show distinct positive excursions of 1–1.5‰ locally alongside qualitative measures of

408 cooling, such as changes in the direction of foraminiferal coiling (Grosheny et al., 2017; Gale et
409 al., 2019).

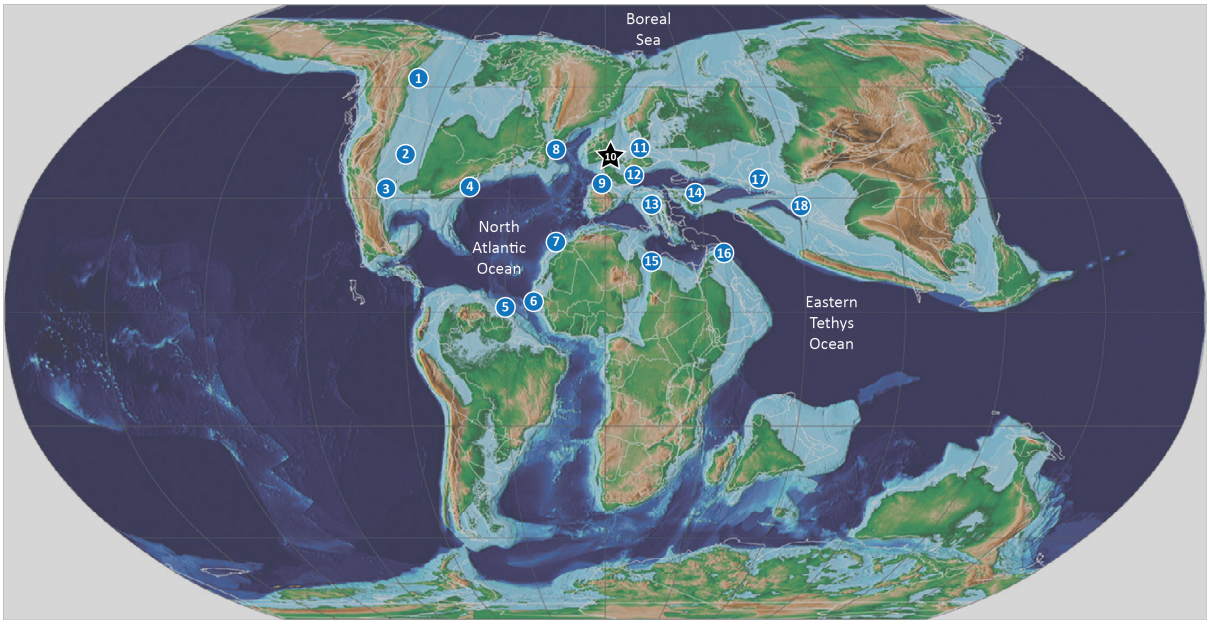

410

411 **Figure 6.** Global distribution of known records demonstrating a change in temperature across the
412 PCE interval, based on records of TEX_{86}, $\delta^{18}O$, faunal assemblages, and foraminiferal coiling. **1**
413 Pratt's Landing (van Helmond et al., 2016). **2** Hot Springs, SD (Desmares et al., 2016); Pueblo
414 (Caron et al., 2006; Desmares et al., 2016); USGS Portland-1 Core (Eldrett et al., 2017). **3** Iona-1
415 core, Innes-1 core, Well X core (Eldrett et al., 2017). **4** Bass River, NJ (van Helmond et al.,
416 2013). **5** ODP Site 1260 (Forster et al., 2007; Eldrett et al., 2017). **6** DSDP Site 367 (Forster et
417 al., 2007). **7** Tarfaya (Tsikos et al., 2004; Kuhnt et al., 2017). **8** ODP Site 1276 (Sinninghe
418 Damsté et al., 2008). **9** Arobes, Ganuza, Menoyo (Kaiho et al., 2014); Puentedey (Barroso-
419 Barcenilla et al., 2011). **10** Dover (this study; Jefferies 1962; Jeans et al., 1991; Lamolda et al.,
420 1994); Eastbourne (Jenkyns et al., 1994; Paul et al., 1999; Tsikos et al., 2004; Voigt et al., 2004,
421 2006; Pearce et al., 2009; Zheng et al., 2013). **11** Gröbern (Voigt et al., 2006); Halle (Voigt et al.,
422 2007); Wunstorf (van Helmond et al., 2015). **12** Cassis (Heimhofer et al., 2018); Clot Chevalier

(Gale et al., 2019); Lambruisse (Takashima et al., 2009); les Lettes (Gale & Christensen 1996); Pont d'Issole (Jarvis et al., 2011). **13** Gubbio (Jenkyns et al., 1994). **14** Crimea (Fisher et al., 2005). **15** Oued Mellegue (Nederbragt & Fiorentino 1999); Wadi Bahoul (Caron et al., 2006). **16** Wadi Karak (Farouk et al., 2017). **17** Amaki, Khadzhalmakhi, Levashi (Gavrilov et al., 2013). **18** Taherabad (Kalanat et al., 2018).

Although cooling appears to be geographically widespread, the precise timing of the falls in local paleotemperature is not consistent globally, or even within a single basin. For example, in Germany, Pueblo and DSDP Site 367, cooling starts well before the P-CIE and reaches its lowest temperature around point 'a', based on TEX_{86}, $\delta^{18}O$, foraminiferal coiling, and faunal assemblages (Figure 7; Voigt et al., 2007; Forster et al., 2007; van Helmond et al., 2015; Desmares et al., 2016). By contrast, in the Chalk records from southern England, and TEX_{86} records from DSDP Site 367 (Equatorial Atlantic) and ODP Site 1276 (North Atlantic), the cooling apparently started later and peaked around point 'b' (Lamolda et al., 1994; Gale and Christensen, 1996; Forster et al., 2007; Sinninghe Damsté et al., 2010). Other sites, such as Tarfaya and ODP Site 1260 suggest a more complex pattern of cooling, with multiple excursions in the TEX_{86} and $\delta^{18}O$ records (Forster et al., 2007; Kuhnt et al., 2017). However, Tarfaya is recognized as a paleo-upwelling area, which would have complicated the SST response (e.g. Einsele and Wiedmann, 1982; Kolonic et al., 2005). Although local diagenesis may have affected some of the SST records, in particular those deriving from oxygen isotopes, the existence of consistent differences in the relative timing between carbon-isotope events and local paleotemperature minima (based on both geochemical and paleontological proxies) suggests that the cooling of water-masses was diachronous.

446

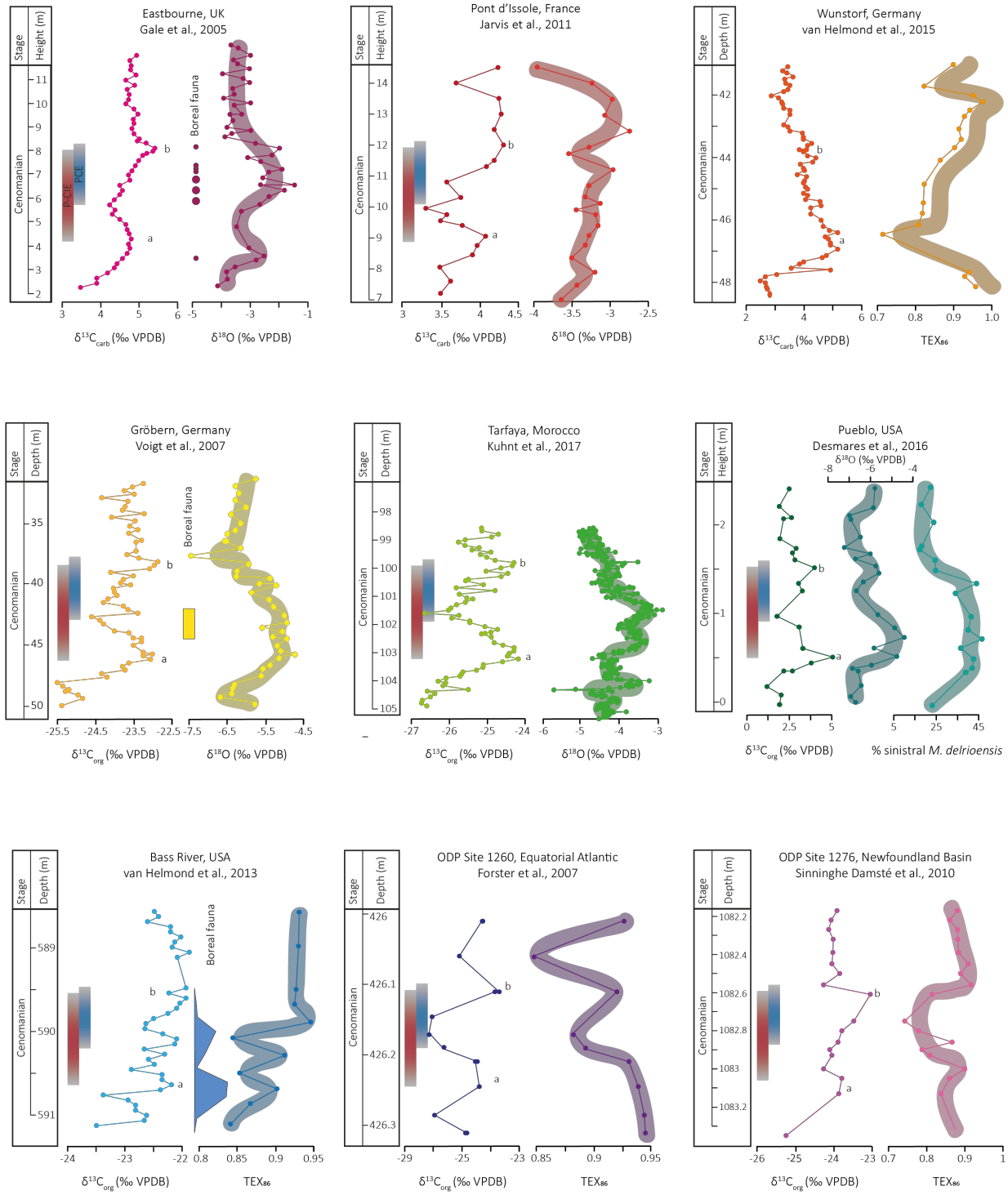
Eastbourne, UK
Gale et al., 2005
Pont d'Issole, France
Jarvis et al., 2011
Wunstorf, Germany
van Helmond et al., 2015
Gröbern, Germany
Voigt et al., 2007
Tarfaya, Morocco
Kuhnt et al., 2017
Pueblo, USA
Desmares et al., 2016
Bass River, USA
van Helmond et al., 2013
ODP Site 1260, Equatorial Atlantic
Forster et al., 2007
ODP Site 1276, Newfoundland Basin
Sinninghe Damsté et al., 2010
Stage
Height (m)
Depth (m)
Cenomanian
P-CIE
PCE
Boreal fauna
δ13Ccarb (‰ VPDB)
δ18O (‰ VPDB)
δ13Corg (‰ VPDB)
TEX86
% sinistral M. delrioensis

447

448 **Figure 7.** Records of SSTs during the Plenus interval. The gray boxes indicate the OAE 2
449 interval; the red boxes indicate the P-CIE; the blue boxes indicate the PCE *sensu stricto*; points
450 'a' to 'c' of the OAE are labelled. Dover stratigraphy from Lamolda et al., 1994; Wunstorf
451 stratigraphy from Voigt et al., 2008. Coloured bands illustrate visual approximations of trends.

452

453 4.2 Evidence for changing water-mass character

454 Geochemical, lithological, and faunal records across OAE 2 demonstrate significant and
455 variable changes in water-mass character associated with the event, variously attributed to
456 changes in redox, circulation, and/or volcanic activity (Figure 8; e.g. Eicher and Worstell, 1970;
457 Orth et al., 1993; MacLeod et al., 2008; Martin et al., 2012; Thomas & Tilghman 2014).
458 However, few records are of sufficiently high resolution to both identify the Plenus interval and
459 any oceanographic changes associated therewith and determine the precise cause of these
460 changes.

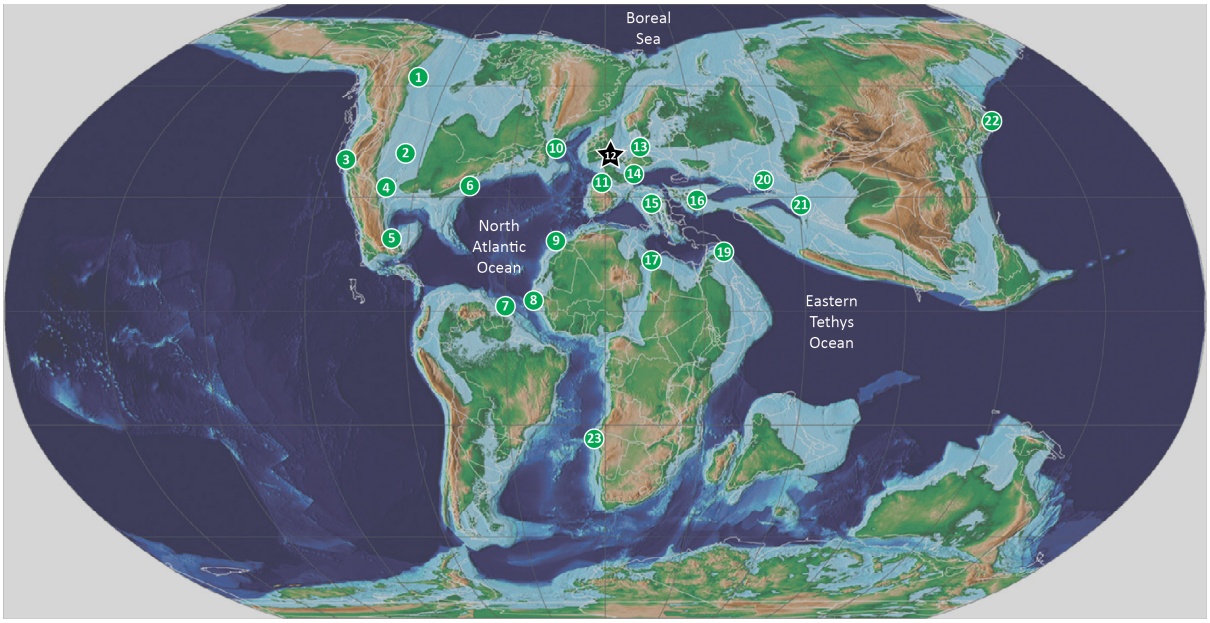

461

462 **Figure 8.** Global distribution of known records demonstrating a change in water-mass character
463 across the Plenus interval, as indicated by elemental, isotopic, lithological, or faunal changes in
464 the sedimentary record. **1** Vermillion River (Prokoph et al., 2013). **2** Angus Aristocrat core
465 (Zhou et al., 2015); Cuba, KS (Bowman & Bralower 2015; Elderbak et al., 2014); Hot Springs,
466 SD (Desmares et al., 2016); USGS Portland-1 core (Du Vivier et al., 2014; Holmden et al., 2016;
467 Eldrett et al., 2017); generalized Western Interior Seaway (Orth et al., 1993); Pueblo (Bowman
468 & Bralower, 2005; Caron et al., 2006; Keller et al., 2008; Elderbak et al., 2014). **3** Great Valley
469 Sequence, CA (Du Vivier et al., 2015). **4** Innes-1 core, Iona-1 core, Well X core (Eldrett et al.,
470 2017). **5** Barranco el Canon (Elrick et al., 2009; Sweere et al., 2018). **6** Bass River, NJ (Bowman
471 and Bralower, 2005). **7** ODP Site 1258 (Erbacher et al., 2005; Friedrich et al., 2006; Ostrander et
472 al., 2017; Zhou et al., 2015); ODP Site 1260 (Erbacher et al., 2005; Friedrich et al., 2006; Forster
473 et al., 2007; Turgeon and Creaser, 2008; Du Vivier et al., 2014; Eldrett et al., 2017); ODP Site
474 1261 (Erbacher et al., 2005; Friedrich et al., 2006). **8** DSDP Site 367 (Kuypers et al., 1999;
475 Forster et al., 2007, 2008; Sinninghe Damsté et al., 2008; Du Vivier et al., 2014; Dickson et al.,
476 2016). **9** Tarfaya (Kuypers et al., 2002; Tsikos et al., 2004; Keller et al., 2008; Dickson et al.,
477 2016; Kuhnt et al., 2017); Mpl, S13, S57, S75 (Kolonic et al., 2005). **10** ODP Site 1276
478 (Sinninghe Damsté et al., 2008; van Helmond et al., 2014). **11** Puentedey (Barroso-Barcenilla et
479 al., 2011); Arobes (Kaiho et al., 2014); Ganuza (Peryt and Lamolda, 1995; Kaiho et al., 2014);
480 Manivala (Mort et al., 2007); Menoyo (Peryt and Lamolda, 1995; Kaiho et al., 2014). **12** Dover
481 (this study; Jeans et al., 1991); Eastbourne (Orth et al., 1993; Paul et al., 1999; Pearce et al.,
482 2009; Lu et al., 2010; Owens et al., 2013; Zheng et al., 2013; Zhou et al., 2015; Clarkson et al.,
483 2018; Sweere et al., 2018). **13** Wunstorf (van Helmond et al., 2015); Halle (Voigt et al., 2007);
484 Roter Sattel (Charbonnier et al., 2018); Wunstorf (Du Vivier et al., 2014; van Helmond et al.,

2015). **14** Clot Chevalier (Gale et al., 2019); Lambruisse (Takashima et al., 2009); Le Bourgeut (Grosheny et al., 2017); Pont d'Issole (Grosheny et al., 2006; Jarvis et al., 2011; Danzelle et al., 2018); Vocontian Basin (Du Vivier et al., 2014). **15** Bottaccione (Kuroda et al., 2007); Furlo (Mort et al., 2007); Gubbio (Tsikos et al., 2004); Raia del Pedale (Owens et al., 2013; Zhou et al., 2015; Clarkson et al., 2018; Sweere et al., 2018). **16** Crimea (Fisher et al., 2005). **17** Oued Mellegue (Nederbragt & Fiorentino 1999); Wadi Bahoul (Caron et al., 2006). **18** Wadi Feiran (El-Sabbagh et al., 2011). **19** Wadi Karak (Farouk et al., 2018). **20** Aimaki, Khadzhalmakhi, Levashi (Gavrilov et al., 2013). **21** Gharesu (Kalanat et al., 2016); Taherabad (Kalanat et al., 2016, 2017). **22** Tappu (Nemoto & Hasegawa 2011); Yezo Group (Du Vivier et al., 2015). **23** DSDP Site 530 (Forster et al., 2008; Du Vivier et al., 2014). **24** Gongzha (Bomou et al., 2013).

Chromium is a redox-sensitive metal that may also be derived from basalt–seawater interactions, and as such is a useful tool for tracking changes in seawater chemistry (e.g. Bonnand et al., 2013; Holmden et al., 2016; Remmelzwaal et al., 2019). At Dover in SW England, carbonate-fraction Cr concentrations show a ~5-fold increase over the uppermost marls (this study; Figure 2). Similar spikes in geochemical species (such as Cr, Mo, U, Mn) have been recorded at sites in the Chalk Sea and/or along the Tethyan margins (e.g. Orth et al., 1993; Jarvis et al., 2001; Kolonic et al., 2005; Pearce et al., 2009; Jenkyns et al., 2017; Charbonnier et al., 2018; Clarkson et al., 2018; Danzelle et al., 2018; Sweere et al., 2018; Gale et al., 2019), North Atlantic (van Helmond et al., 2014; Dickson et al., 2016; Eldrett et al., 2017) and the Western Interior Seaway (Orth et al., 1993; Holmden et al., 2016; Eldrett et al., 2017). These excursions have been attributed to a period of increased bottom-water oxygenation during which the remineralisation of organic-matter either released trace metals into the water column and/or

508 removed anoxic/euxinic sinks for hydrothermally enriched bottom waters (Jenkyns et al., 2017).
509 However, some sites show excursions in certain geochemical species but not others (e.g. Owens
510 et al., 2013; Eldrett et al., 2017; Danzelle et al., 2018; Sweere et al., 2018). These differences
511 may be due to the different reduction potentials of various elements and the local redox
512 conditions pertaining at any one site. Local redox conditions during the Plenus interval may have
513 prevented certain elements from being enriched in discrete reduced phases, such as in sulphides,
514 or substituting in pyrite or adsorbed onto organic matter but not allowed them to be incorporated
515 in carbonates in more oxidized form even if present in relative abundance in
516 seawater. Regardless of the cause, these variable expressions of redox change across the Plenus
517 interval make it difficult to deconvolve global from local drivers of paleoenvironmental change.
518 Neodymium-isotope ratios, expressed as ε_{Nd}, are a powerful tool for reconstructing
519 changes in past ocean circulation (Frank, 2002; Goldstein and Hemming, 2003). Roughly coeval
520 with the Cr excursion in the Chalk of SW England, large (~1.5 ε unit) excursions in neodymium
521 isotopes across the PCE interval suggest changing circulation and/or possible input of
522 magmatically derived radiogenic Nd (this study; Zheng et al., 2013, 2016). A link has been
523 drawn between LIPs and oceanic anoxic events, particularly with respect to the Caribbean and
524 High Arctic Large Igneous Provinces as possible triggers for OAE 2 (e.g. Snow et al., 2005;
525 Tegner et al., 2011; Zheng et al., 2013). Osmium-isotope records from across the world have
526 identified periods of volcanism or some form of basalt–seawater interaction around the
527 Cenomanian–Turonian boundary, indicating likely LIP activity immediately prior to the onset of
528 OAE 2 (Turgeon and Creaser, 2008; Du Vivier et al., 2014, 2015; Scaife et al., 2017; Schröder-
529 Adams et al., 2019). Basalt–seawater interactions would not have just affected seawater Nd and

Os, but also other trace metals and isotopes, which further complicates the interpretation of their sedimentary records.

Ce anomalies reflect the oxidation state of seawater through the oxidation of Ce (III) to insoluble and particle-reactive Ce (IV) (De Baar et al., 1988; Zhou et al., 2016; Remmelzwaal et al., 2019). In the Dover record, Ce* steadily decreases up-section, mirroring the generally increasing pattern of $\delta^{13}C$. These data can be compared with trace-element data from the Eastbourne section (Lu et al., 2010; Jenkyns et al., 2016). Cerium anomalies at Dover are generally lower during the PCE than prior to the event, but there is a significant increase in Ce/Ce* from 0.7 to 0.83 at the beginning of the OAE event in the Dover section. This rise is consistent with Mn/Ca data for the Eastbourne section, suggestive of an initial move to a less oxic sub-seafloor, whereas the overall decrease in Ce/Ce*, particularly during the PCE is consistent with I/Ca ratios indicating a move to more oxic surface waters at this time (Lu et al., 2010). Seawater and carbonates in modern marine environments commonly have both Ce and La anomalies and this is best demonstrated by calculating Ce/Ce* and Pr/Pr* values, which also co-vary with each other (Webb and Kamber, 2000). Our new carbonates record indicates that the late Cenomanian seawater also has both Ce and La anomalies. While Ce/Ce* and Pr/Pr* (not shown) values vary smoothly through the section, they are principally indicative of variable redox conditions, whereas La/Pr ratios still retain information about source input and are much more variable. In this case, the La/Pr ratio is a useful guide to the amount of basaltic input to the seawater because average altered basaltic crust has La/Pr value of 1.65 (Kelley et al, 2003) whereas the upper continental crust has a value of 4.37 (Rudnick and Gao, 2003). Therefore, lower La/Pr ratios are indicative of an increased basaltic input, either from basalt–seawater interaction or re-oxygenation of sea-floor sediment. La/Pr ratios decrease at the beginning of the

OAE level and during the interval of the two cooling events, particularly the main PCE, at which level it is consistent with positive shifts in Nd isotopes.

Re-oxygenation of bottom water has also been invoked as the cause of decreased TOC in Plenus records from the Tethys, North Atlantic, and even Japan (Tsikos et al., 2004; Bowman & Bralower 2005; Forster et al., 2007; Sinninghe Damsté et al., 2010; Jarvis et al., 2011; Nemoto & Hasegawa 2011; van Helmond et al., 2013, 2014; Eldrett et al., 2014, 2017; Dickson et al., 2016; Kunht et al., 2017). However, many sites record no change in the TOC, or in some cases an increase, suggesting locally sustained bottom-water oxygenation or simply changes in productivity (e.g. Kuypers et al., 2002; Tsikos et al., 2004; Kolonic et al., 2005; Mort et al., 2007; Gavrilov et al., 2013; Dickson et al., 2016; Kuhnt et al., 2017).

Faunal records showing an increase in benthic organisms and bioturbation during the Plenus interval suggest increased bottom-water oxygenation at sites across the Chalk Sea of northern Europe (Jarvis et al., 1988; Peryt and Lamolda, 1995; Paul et al., 1999; Takashima et al., 2009), Tethyan margin (Barroso-Barcenilla et al., 2011; Kalanat et al., 2016), North Atlantic (Eldrett et al., 2017), and Western Interior Seaway (Desmares et al., 2007; Elderbak et al., 2014). However, as with the TOC records, some sites show no change in benthic faunal abundance over this interval, or in some cases a decrease, further suggesting locally sustained bottom-water anoxia (e.g. Grosheny et al., 2006, 2017; Friedrich et al., 2006; Keller et al., 2008; El-Sabbagh et al., 2011).

Trace-metal, isotope, TOC, and faunal records all suggest pockets of re-oxygenation, but it remains difficult to link these directly to global changes in the carbon cycle or temperature. Furthermore, different water depths at different sites will have directly influenced bottom-water oxygenation, and may determine whether anoxia could have occurred in the first place.

576

577 **5 Implications for understanding environmental changes during the Plenus Cold Event**

578 5.1 Carbon-cycle perturbation

579 The remarkable consistency of the carbon-isotope signature of OAE 2 across the globe
580 allows for chemostratigraphic correlation of the event, albeit with the caveat that variable
581 organic-matter sources can affect bulk $\delta^{13}C_{org}$ and variable diagenesis can affect $\delta^{13}C_{carb}$,
582 particularly in sediments containing potentially reactive organic matter.

583 In a comparison of bio- and chemostratigraphy of OAE 2 between Europe and North
584 America, Gale et al. (1993) found a consistent relationship between the two, which these authors
585 took as evidence for effective synchroneity between certain paleontological markers and the
586 carbon-isotope events in Europe and North America (despite some endemism and preservation
587 problems, particularly associated with facies changes). More recent and higher-resolution studies
588 support this contention, namely global parallels in the general patterns of microfossil and
589 macrofossil biostratigraphy and $\delta^{13}C$ correlations (Jarvis et al., 2006; Wendler 2013). These
590 records indicate a globally synchronous response of the bio- and chemostratigraphic record to the
591 OAE, and that the characteristic carbon-isotope signature can be reliably used in correlation.

592 The terrestrially derived CO_2 records and the majority of marine CO_2 records show a rise
593 then fall in atmospheric CO_2 across the P-CIE, suggesting a global carbon-cycle event. As such,
594 we propose that the negative $\delta^{13}C$ excursion could—and should—be used as a stratigraphic
595 marker to identify the Plenus interval in local archives. This approach to stratigraphic correlation
596 avoids potential miscorrelation issues caused by possible diachroneity of any cooling observed at
597 different locations, which could have been impacted by the local oceanographic conditions.

598 The driver of this CO_2 change is more difficult to identify. Initially it was proposed that
599 increased organic-carbon burial during the initial stages of OAE 2 drove a drawdown of
600 atmospheric CO_2 (Arthur et al., 1988; Freeman & Hayes 1992; Jenkyns et al., 1994; Kuypers et
601 al., 1999; Forster et al., 2007; Sinninghe Damsté et al., 2010; Jarvis et al., 2011). Therefore, an
602 increase in bottom-water re-oxygenation during the Plenus interval would have led to a
603 temporary reduction of organic-matter deposition and/or the remineralisation of sedimentary
604 carbon on the sea floor, driving an increase in CO_2. The Cenomanian–Turonian boundary was
605 also a period of enhanced basalt–seawater interaction owing to the emplacement of at least two
606 large igneous provinces (LIPs): the Caribbean Large Igneous Province (CLIP; Snow et al., 2005)
607 and the High Arctic Large Igneous Province (HALIP; Tegner et al., 2011; Davis et al., 2017;
608 Kingsbury et al., 2018; Schröder-Adams et al., 2019). A cessation of this outgassing may have
609 resulted in an overall decrease in pCO_2 (e.g. Turgeon & Creaser, 2008; Du Vivier et al., 2014,
610 2015; Scaife et al., 2017). Indeed, Kuroda et al. (2007) suggested, based on a coeval shift in Pb
611 isotopes indicative of an increase in hydrothermal input of Pb, that the negative carbon-isotope
612 excursion observed during the Plenus interval reflects an increase in pCO_2 due to volcanism,
613 rather than a drop in global burial rates of organic carbon. The changing balance between CO_2
614 drawdown due to organic-carbon burial versus volcanic and tectonic emissions of this
615 greenhouse gas is difficult to constrain. However, a rise in atmospheric CO_2 would drive an
616 increase in global temperatures—the opposite of what is observed. This apparent mismatch
617 between theory and observation highlights complications in drawing causative links between
618 putative CO_2 levels and the PCE, as it was originally interpreted.

619 5.2 Accompanying climatic phenomena

620 There is a wealth of data indicating widespread paleoenvironmental change during the
621 early stages of OAE 2 but the question remains as to what drove such phenomena in different
622 parts of the globe. Accounting for problems inherent in bio-, chemo-, and lithostratigraphic
623 correlation, the records show little consistency in the timing of temperature and seawater
624 chemistry (Figures 5 and 7). The onset of these changes apparently appeared much earlier at
625 some sites than others, even locally preceding the negative carbon-isotope excursion, suggesting
626 that oceanic processes may have responded to forcing mechanisms other than just changes in
627 ocean–atmosphere pCO_2, such as a change in local circulation, productivity, or basalt–seawater
628 interactions.

629 5.3.1 Changing water-mass character

630 A change in circulation, bottom-water re-oxygenation, and basalt–seawater interactions
631 have variously been proposed to drive the excursions seen in different proxy records discussed in
632 Section 4.3. However, records of seawater chemistry are difficult to interpret as the proxies may
633 have responded to more than one process, or one process may have driven another. The
634 neodymium-isotopic signal of a water-mass may reflect changes in circulation, but it can also be
635 affected by basalt–seawater interaction introducing radiogenic Nd. Although complicating the
636 interpretation of ε_{Nd} records, the geochemical imprint of basalt on seawater may be helpful for
637 tracing the source of a water-mass to volcanically affected areas.

638 The positive ε_{Nd} excursion in the Eastbourne record was interpreted by Zheng et al.
639 (2016) to reflect the input of strongly radiogenic Nd from volcanism through relatively oxygen-
640 poor water, citing the coeval emplacement of the Caribbean Large Igneous Province (Snow et
641 al., 2005) and the High Arctic Large Igneous Province (Tegner et al., 2011; Davis et al., 2017;

642 Kingsbury et al., 2018). Due to the lack of outcrop, the chemistry and eruption history of these
643 LIPs are poorly constrained, which makes it difficult to pinpoint the source of any volcanically
644 derived radiogenic Nd. For CLIP to have acted as the source of radiogenic Nd would have
645 required transfer of the geochemical bottom-water signal from the Pacific Ocean to southern
646 England across the eastern paleo-Pacific and proto-Atlantic (cf. Trabucho Alexandre et al.,
647 2010). Given that the residence time of neodymium in the ocean today is roughly equal to the
648 mixing time of the ocean (Frank, 2002; Goldstein & Hemming 2003; Thomas 2005), CLIP-
649 derived radiogenic Nd is unlikely to have induced such a large positive shift in ε_{Nd} in such a
650 distal location as southern England. Neodymium might have had a longer residence time in
651 relatively deoxygenated seawater because Fe-Mn oxyhydroxides (a sink for Nd) would not have
652 been stable under such conditions (Halliday et al., 1992); however, such conditions would have
653 been less applicable during the apparently more oxygenated conditions (at least in southern
654 England) of the PCE itself. If a water-mass from the vicinity of the HALIP moved south,
655 carrying a radiogenic Nd signature, it could have produced a positive ε_{Nd} excursion while
656 simultaneously causing a drop in water temperature, as seen in the Dover record (Figure 2).
657 Furthermore, as O_2 solubility is dependent on water temperature (e.g. Broecker & Peng 1974), a
658 cold water-mass would have contained higher concentrations of dissolved O_2 compared with
659 warmer waters and could have induced a redox shift in bottom-waters, as suggested by the trace-
660 metal record at Dover (Figure 2) and Eastbourne (Jenkyns et al., 2017).

661 Trace-metal and isotopic excursions have been ascribed to two factors: 1) bottom-water
662 re-oxygenation during the PCE, whereby the remineralisation of trace-metal-rich organic matter
663 deposited during the early stages of the OAE released metals into the water column, some of
664 which were subsequently incorporated into nannofossil and foraminiferal carbonate (Jenkyns et

al., 2017); and 2) alternatively, or additionally, the transient loss of the organic-rich sink during re-oxygenation events during the Plenus interval, with ongoing basalt–seawater interaction continuing to liberate volcanically derived trace metals, allowed their build-up in ocean waters (Orth et al., 1993; Pearce et al., 2009; Holmden et al., 2016; Jenkyns et al., 2017).

Decreased TOC across the Plenus interval has also been suggested to indicate a redox shift (e.g. Tsikos et al., 2004; Jarvis et al., 2011; Eldrett et al., 2014, 2017), although organic-matter content may be affected by changes in preservation, productivity, or dilution. Increased oxygenation of bottom-waters would inhibit the deposition of organic matter, though this assumes a simple coupling between anoxia and organic-matter deposition in the first place, which is manifestly a gross simplification (e.g. Demaison and Moore, 1980; Pedersen and Calvert, 1990). Deposition of the characteristic black shales of OAE 2 was not a global phenomenon, but rather limited to environments that favourably supported organic-matter burial, particularly the Atlantic and Tethyan regions and the equatorial Pacific (Schlanger et al., 1987; Takashimi et al., 2009). Furthermore, local to regional variations in productivity, preservation, sedimentation rate, and seawater chemistry led to differences in the timing of local maxima in organic-carbon burial rates. Particularly in former upwelling areas, such as the western sides of continents or the paleo-Equator, increases in organic productivity, initially unrelated to bottom- or mid-water redox, may have driven an increase in organic-matter deposition. An increased supply of biologically significant metals or minerals may also have resulted directly from basalt–seawater interactions, and/or increased terrestrial weathering, and consequent accelerated fluvial nutrient input to the oceans, which may in turn have driven an expansion of organic productivity (Jenkyns, 2010). Local changes in these processes—whether related or unrelated to global CO_2 and temperature—may have driven either an increase or decrease in organic-matter deposition

that might be misconstrued as a redox shift. These factors may also explain the records of increased TOC across the Plenus interval in Spain (Mort et al., 2007) and Morocco (Kuhnt et al., 2017). Given the enhanced hydrological cycle, proposed to have driven an increase in silicate weathering during the OAE (Blättler et al., 2011; Pogge van Strandmann et al., 2013), changes in terrestrial weathering and sedimentary dilution may also have affected the TOC without changing productivity or preservation.

5.3.1 Cooling

Cooling events are observed across the Northern Hemisphere during the Plenus interval, for which a range of mechanisms has been proposed:

(1) A causal link has been suggested between SSTs and the carbon cycle during OAE 2: at its simplest, the widespread deposition of organic matter during OAE 2 is credited with leading to CO_2 drawdown and, in turn, transient cooling (Arthur et al., 1988; Freeman & Hayes 1992; Jenkyns et al., 1994; Kuypers et al., 1999; Forster et al., 2007; Sinninghe Damsté et al., 2010; Jarvis et al., 2011). However, if these temperature records (TEX_{86}, $\delta^{18}O$, fauna) were solely recording the SST response to global atmospheric cooling, they would be expected to show a degree of synchroneity and expression: cooling occurring *during and after* the CO_2 decrease, during the later phase of the P-CIE close to point 'b' (e.g. scenario (1) in Figure 9; Eastbourne and ODP Site 1276 in Figure 7). While a global decrease in temperatures would have been a necessary response to falling atmospheric CO_2 levels, the SST records—if accepted at face value—show significant variability in the timing of the cooling relative to the P-CIE. The TEX_{86}, $\delta^{18}O$, and faunal records that show cooling preceding the CO_2 decrease, in the early phase of the P-CIE close to point 'a' (e.g. Wunstorf, Gröbern, Bass River, Pueblo; Figure 7), which implies either an indirect response of local SSTs to CO_2 change, or simply the effect of

711 local oceanographic conditions independent of global change. Furthermore, it is difficult to
712 directly link the cooling seen at point 'b' to global processes, when the drop in temperature may
713 have been due to a circulation change bringing cooler water to a locality (as seen by the
714 simultaneous cooling and Nd excursion in SE England) (Figures 2 and 9).

715 (2) Ocean circulation is thought to have been a critical component of the climate system
716 during the Plenus interval, wherein CO_2 drawdown led to global cooling and increased latitudinal
717 temperature gradients, which in turn drove a change in circulation (Zheng et al., 2013; van
718 Helmond et al., 2014; Eldrett et al., 2017). However, there are two problems with this
719 hypothesis. Firstly, as in (1), this model does not account for cooling preceding the CO_2
720 decrease. Secondly, if global cooling drove the circulation change, one would expect one phase
721 of cooling after the CO_2 change then another after the circulation change, but none of the records
722 show this. As such, this model cannot account for cooling in the early phase of the P-CIE, close
723 to point ‘a’, which indicates that CO_2-driven circulation change was not a direct driver of the
724 cooling at all sites.

725 (3) Alternatively, circulation might have been altered due to factors unrelated to global
726 temperatures and latitudinal gradients, perhaps owing to changes in upwelling (e.g. Einsele and
727 Wiedmann 1982; Kolonic et al., 2005), deepening and shallowing of local sea levels affecting
728 upper-ocean circulation patterns (e.g. Hancock, 1993; Voigt and Wiese, 2000; Voigt et al.,
729 2006), or LIP-related tectonics (e.g. Maher 2001; Dostal & MacRae 2018). These changes in
730 circulation may have brought cooler water-masses to regions bordering the Arctic, producing a
731 decrease in local SSTs. Within the Chalk Sea and the Western Interior Seaway, rises in $\delta^{13}C$
732 correlate with local transgressions (Voigt and Hillbrecht, 1997; Voigt and Wiese, 2000; Laurin et
733 al., 2019). The timing of the cooling and circulation change observed in the Chalk Sea of

734 southern England is coincident with the rising limb of the P-CIE and evidence for a local
735 transgression, suggesting deepening of the sea may have allowed an ingress of cooler boreal
736 waters.

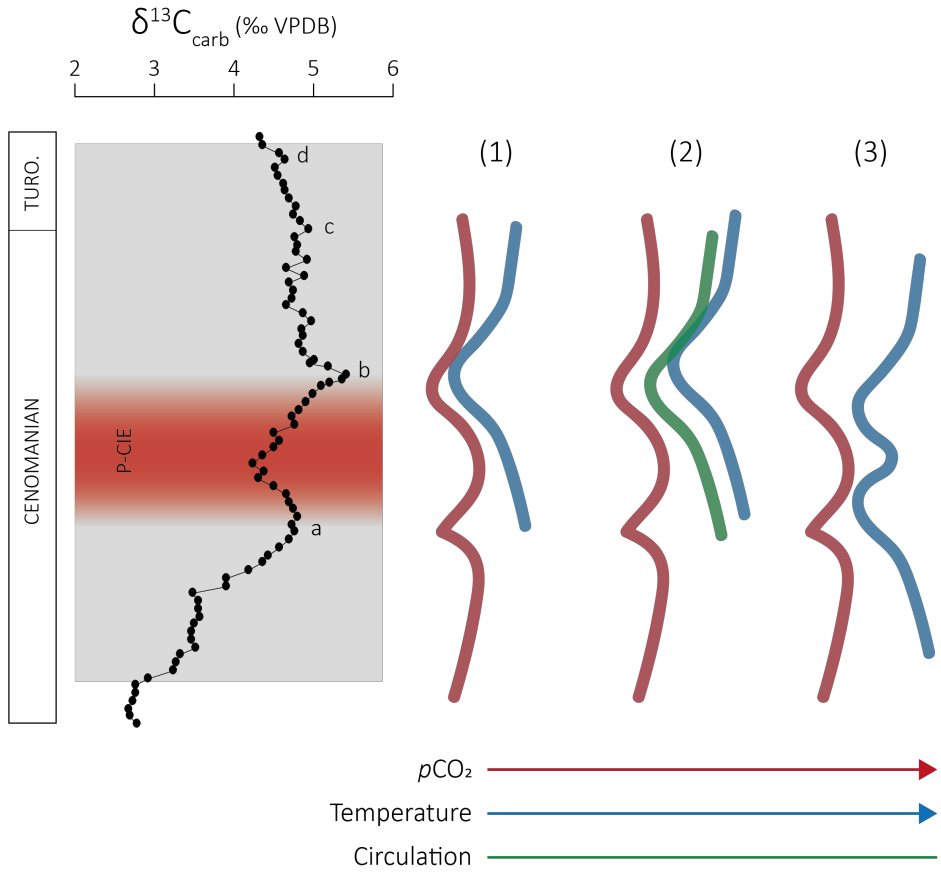

737

738 **Figure 9.** Potential models for cooling during the PCE. $\delta^{13}C$ from Eastbourne (Tsikos et al.,
739 2004). The gray box indicates the OAE 2 interval; the red box indicates the P-CIE; points 'a' to
740 'd' of the $\delta^{13}C$ curve are labelled. The red lines indicate CO_2, the blue lines indicate SST, and the
741 green line indicates circulation. Values are arbitrary. Model (1): a direct link between CO_2,
742 atmospheric temperatures, and SSTs would produce a cooling interval after a drop in CO_2.
743 Model (2): a fall in CO_2 would drive global temperature decrease, forcing a circulation change
744 and, in turn, further cooling. In this model, cooling must come after the CO_2 change. Model (3):

745 no direct link between CO_2 and SSTs would produce variable timing and expression of
746 temperatures at individual sites.
747
748 Although OAE 2 was a period of extreme global climate perturbation, the local
749 temperature responses to increased CO_2 likely varied in magnitude, trend and, potentially, sign.
750 Thus, interactions between climatic and oceanographic processes may account for the different
751 expressions of cooling seen at different sites, especially the cooling seen in the early stages of the
752 P-CIE. If nothing else, the apparent diachroneity in cooling highlights the problems associated
753 with using any local expression of temperature or water-mass character during the Plenus
754 interval as a correlation tool or stratigraphic marker.
755

756 5. Conclusions

757 The Cenomanian–Turonian transition experienced extreme climate change and major
758 volcanic and tectonic activity. The increase in silicate weathering due to an enhanced
759 hydrological cycle on the continents and the weathering of LIP-related basalts in the oceans
760 probably drove a drawdown in CO_2, as did high rates of organic-carbon burial. The on-going
761 basalt–seawater interaction, likely concentrated in the first half of OAE 2 based on regional
762 osmium-isotope signatures (Du Vivier et al., 2014, 2015), would have further affected both
763 atmospheric pCO_2 and global carbon-isotope compositions. In contrast, volcanic outgassing and
764 the cessation of organic-carbon deposition would have driven an *increase* in pCO_2. However, it
765 is not possible to disentangle these processes and their effects on the carbon cycle from the
766 current data.

During the Plenus interval, there is evidence for widespread environmental change across the Northern Hemisphere. The global extent of negative $\delta^{13}C$ excursions, coincident with records of increasing pCO_2, suggest an increase in atmospheric CO_2 and a global carbon-cycle event—the Plenus CIE. However, the records of cooling show no consistency in timing or expression, and suggest either that some or all of the proxy records are compromised by diagenesis or environmental factors, and/or there was no clear-cut link between SSTs and atmospheric pCO_2. While there was likely a global fall in temperatures relating to the drop in CO_2, applying simple cause-and-effect relationships between CO_2 and temperature does not explain all observations. Furthermore, variability in the timing and expression of changes in seawater chemistry, and problems in determining the driver of observed proxy changes, suggests that no one simple mechanism can link the carbon cycle to oceanography during the Plenus interval. While these stratigraphic offsets do not contradict the hypothesis of a global pCO_2 decrease directly driving cooling with a concomitant or subsequent change in ocean circulation, they do suggest that local effects played a modifying role on the local timing and expression of events. To advance the understanding of the Plenus event, more geographically widespread records are required, ideally with proxies for temperature, CO_2, and ocean circulation applied in a single setting.

Given the global nature of the negative $\delta^{13}C$ excursion and the decrease in atmospheric pCO_2, it is proposed that the Plenus CIE is a more reliable stratigraphic marker to identify the stratigraphic interval during which local expressions of the Plenus interval were developed with or without evidence for a fall in temperature and/or a drop in pCO_2.

Acknowledgments, Samples, and Data

The authors would like to thank Alan Hseih, Chris Day, and Steve Wyatt for their technical assistance at the Department of Earth Sciences, University of Oxford. L.K.O. would like to thank

790 the Clarendon Fund (University of Oxford) and University College, Oxford, for supporting her
791 DPhil. S.R.C.R would like to thank NERC GW4+ for his studentship. Data are available in the
792 supplement and at https://doi.pangaea.de/10.1594/PANGAEA.909150

793

794 **References**

795 Arthur, M. A., Brumsack, H.-J., Jenkyns, H. C., & Schlanger, S. O. (1990). Stratigraphy,
796 Geochemistry, and Paleoceanography of Organic Carbon-Rich Cretaceous Sequences.
797 Cretaceous Resources, Events and Rhythms, 75–119. https://doi.org/10.1007/978-94-015-6861-
798 6_6

799 Arthur, M. A., Dean, W. E., & Claypool, G. E. (1985). Anomalous ^{13}C enrichment in
800 modern marine organic carbon. Nature, 315(6016), 216–218. https://doi.org/10.1038/315216a0

801 Arthur, M. A., Dean, W. E., & Pratt, L. M. (1988). Geochemical and climatic effects of
802 increased marine organic carbon burial at the Cenomanian/Turonian boundary. Nature,
803 335(6192), 714–717. https://doi.org/10.1038/335714a0

804 Barclay, R. S., McElwain, J. C., & Sageman, B. B. (2010). Carbon sequestration activated
805 by a volcanic CO_2 pulse during Ocean Anoxic Event 2. Nature Geoscience, 3(3), 205–208.
806 https://doi.org/10.1038/ngeo757

807 Barroso-Barcenilla, F., Pascual, A., Peyrot, D., & Rodríguez-Lázaro, J. (2011). Integrated
808 biostratigraphy and chemostratigraphy of the upper Cenomanian and lower Turonian succession
809 in Puentedey, Iberian Trough, Spain. Proceedings of the Geologists' Association, 122(1), 67–81.
810 https://doi.org/10.1016/j.pgeola.2010.11.002

811 Berger, W. H., & Vincent, E. (1986). Deep-sea carbonates: Reading the carbon-isotope

signal. Geologische Rundschau, 75(1), 249–269. https://doi.org/10.1007/bf01770192

Blättler, C. L., Jenkyns, H. C., Reynard, L. M., & Henderson, G. M. (2011). Significant increases in global weathering during Oceanic Anoxic Events 1a and 2 indicated by calcium isotopes. Earth and Planetary Science Letters, 309(1–2), 77–88. https://doi.org/10.1016/j.epsl.2011.06.029

Bomou, B., Adatte, T., Tantawy, A. A., Mort, H., Fleitmann, D., Huang, Y., & Föllmi, K. B. (2013). The expression of the Cenomanian–Turonian oceanic anoxic event in Tibet. Paleogeography, Paleoclimatology, Paleoecology, 369, 466–481. https://doi.org/10.1016/j.paleo.2012.11.011

Bowman, A. R., & Bralower, T. J. (2005). Paleoceanographic significance of high-resolution carbon isotope records across the Cenomanian–Turonian boundary in the Western Interior and New Jersey coastal plain, USA. Marine Geology, 217(3–4), 305–321. https://doi.org/10.1016/j.margeo.2005.02.010

Broecker, W. S., & Peng, T.-H. (1974). Gas exchange rates between air and sea. Tellus, 26(5), 21–35. https://doi.org/10.3402/tellusa.v26i5.9869

Caron, M., Dall'Agnolo, S., Accarie, H., Barrera, E., Kauffman, E. G., Amédro, F., & Robaszynski, F. (2006). High-resolution stratigraphy of the Cenomanian–Turonian boundary interval at Pueblo (USA) and wadi Bahloul (Tunisia): stable isotope and bio-events correlation. Geobios, 39(2), 171–200. https://doi.org/10.1016/j.geobios.2004.11.004

Charbonnier, G., Adatte, T., Spangenberg, J. E., & Föllmi, K. B. (2018). The expression of early Aptian to latest Cenomanian oceanic anoxic events in the sedimentary record of the Briançonnais domain. Global and Planetary Change, 170, 76–92.

https://doi.org/10.1016/j.gloplacha.2018.08.009

Clarkson, M. O., Stirling, C. H., Jenkyns, H. C., Dickson, A. J., Porcelli, D., Moy, C. M., et al., (2018). Uranium isotope evidence for two episodes of deoxygenation during Oceanic Anoxic Event 2. Proceedings of the National Academy of Sciences, 115(12), 2918–2923. https://doi.org/10.1073/pnas.1715278115

Corfield, R. M., Hall, M. A., & Brasier M. D. (1990). Stable isotope evidence for foraminiferal habitats during the development of the Cenomanian/Turonian ocean anoxic event. Geology, 18 (2), 175–178. https://doi.org/10.1130/0091-7613(1990)018<0175:SIEFFH>2.3.CO;2

Damsté, J. S. S., Kuypers, M. M. M., Pancost, R. D., & Schouten, S. (2008). The carbon isotopic response of algae, (cyano)bacteria, archaea and higher plants to the late Cenomanian perturbation of the global carbon cycle: Insights from biomarkers in black shales from the Cape Verde Basin (DSDP Site 367). Organic Geochemistry, 39(12), 1703–1718. https://doi.org/10.1016/j.orggeochem.2008.01.012

Danzelle, J., Riquier, L., Baudin, F., Thomazo, C., & Pucéat, E. (2018). Oscillating redox conditions in the Vocontian Basin (SE France) during Oceanic Anoxic Event 2 (OAE 2). Chemical Geology, 493, 136–152. https://doi.org/10.1016/j.chemgeo.2018.05.039

Davis, W. J., Schröder-Adams, C. J., Galloway, J. M., Herrle, J. O., & Pugh, A. T. (2016). U–Pb geochronology of bentonites from the Upper Cretaceous Kanguk Formation, Sverdrup Basin, Arctic Canada: constraints on sedimentation rates, biostratigraphic correlations and the late magmatic history of the High Arctic Large Igneous Province. Geological Magazine, 154(04), 757–776. https://doi.org/10.1017/s0016756816000376

Demaison, G. J., & Moore, G. T. (1980). Anoxic environments and oil source bed genesis. Organic Geochemistry, 2(1), 9–31. https://doi.org/10.1016/0146-6380(80)90017-0

Desmares, D., Crognier, N., Bardin, J., Testé, M., Beaudoin, B., & Grosheny, D. (2016). A new proxy for Cretaceous paleoceanographic and paleoclimatic reconstructions: Coiling direction changes in the planktonic foraminifera Muricohedbergella delrioensis. Paleogeography, Paleoclimatology, Paleoecology, 445, 8–17. https://doi.org/10.1016/j.paleo.2015.12.021

Desmares, D., Grosheny, D., Beaudoin, B., Gardin, S., & Gauthier-Lafaye, F. (2007). High resolution stratigraphic record constrained by volcanic ash beds at the Cenomanian–Turonian boundary in the Western Interior Basin, USA. Cretaceous Research, 28(4), 561–582. https://doi.org/10.1016/j.cretres.2006.08.009

Dickson, A. J., Jenkyns, H. C., Porcelli, D., van den Boorn, S., & Idiz, E. (2016). Basin-scale controls on the molybdenum-isotope composition of seawater during Oceanic Anoxic Event 2 (Late Cretaceous). Geochimica et Cosmochimica Acta, 178, 291–306. https://doi.org/10.1016/j.gca.2015.12.036

Dickson, A. J., Saker□Clark, M., Jenkyns, H. C., Bottini, C., Erba, E., Russo, F., et al. (2017). A Southern Hemisphere record of global trace-metal drawdown and orbital modulation of organic□matter burial across the Cenomanian–Turonian boundary (Ocean Drilling Program Site 1138, Kerguelen Plateau). Sedimentology, 64(1), 186–203. https://doi.org/10.1111/sed.12303

Dostal, J., & MacRae, A. (2018). Cretaceous basalts of the High Arctic large igneous province at Axel Heiberg Island (Canada): Volcanic stratigraphy, geodynamic setting, and origin. Geological Journal, 53(6), 2918–2934. https://doi.org/10.1002/gj.3132

878 Du Vivier, A. D. C., Selby, D., Condon, D. J., Takashima, R., & Nishi, H. (2015). Pacific
879 $^{187}Os/^{18}$ Os isotope chemistry and U–Pb geochronology: Synchroneity of global Os isotope
880 change across OAE 2. Earth and Planetary Science Letters, 428, 204–216.
881 https://doi.org/10.1016/j.epsl.2015.07.020

882 Du Vivier, A. D. C., Selby, D., Sageman, B. B., Jarvis, I., Gröcke, D. R., & Voigt, S.
883 (2014). Marine $^{187}Os/^{188}Os$ isotope stratigraphy reveals the interaction of volcanism and ocean
884 circulation during Oceanic Anoxic Event 2. Earth and Planetary Science Letters, 389, 23–33.
885 https://doi.org/10.1016/j.epsl.2013.12.024

886 Eicher, D. L., & Worstell, P. (1970). Cenomanian and Turonian Foraminifera from the
887 Great Plains, United States. Micropaleontology, 16(3), 269. https://doi.org/10.2307/1485079

888 Eicher, D.L., and Diner, R., 1985, Foraminifera as indicators of water mass in the
889 Cretaceous Greenhorn sea, Western Interior, *In* Pratt, L.M., Kauffman, E.G., & Zelt, F.B. (Eds.).
890 *Fine-grained deposits and biofacies of the Cretaceous Western Interior Seaway: Evidence of*
891 *cyclic sedimentary processes, Fieldtrip Guidebook* (Vol 4), 60–71. Society of Economic
892 Paleontologists and Mineralogists, Tulsa, Oklahoma. https://doi.org/10.2110/sepmfg.04.060

893 Einsele, G., & Wiedmann, J. (1982). Turonian Black Shales in the Moroccan Coastal
894 Basins: First Upwelling in the Atlantic Ocean? Geology of the Northwest African Continental
895 Margin, 396–414. doi:10.1007/978-3-642-68409-8_16

896 Eldrett, J. S., Dodsworth, P., Bergman, S. C., Wright, M., & Minisini, D. (2017). Water-
897 mass evolution in the Cretaceous Western Interior Seaway of North America and equatorial
898 Atlantic. Climate of the Past, 13(7), 855–878. https://doi.org/10.5194/cp-13-855-2017

899 Eldrett, J. S., Minisini, D., & Bergman, S. C. (2014). Decoupling of the carbon cycle

during Ocean Anoxic Event 2. Geology, 42(7), 567–570. https://doi.org/10.1130/g35520.1

Elrick, M., Molina-Garza, R., Duncan, R., & Snow, L. (2009). C-isotope stratigraphy and paleoenvironmental changes across OAE2 (mid-Cretaceous) from shallow-water platform carbonates of southern Mexico. Earth and Planetary Science Letters, 277(3–4), 295–306. https://doi.org/10.1016/j.epsl.2008.10.020

El-Sabbagh, A., Tantawy, A. A., Keller, G., Khozyem, H., Spangenberg, J., Adatte, T., & Gertsch, B. (2011). Stratigraphy of the Cenomanian–Turonian Oceanic Anoxic Event OAE2 in shallow shelf sequences of NE Egypt. Cretaceous Research, 32(6), 705–722. https://doi.org/10.1016/j.cretres.2011.04.006

Erbacher, J., Friedrich, O., Wilson, P. A., Birch, H., & Mutterlose, J. (2005). Stable organic carbon isotope stratigraphy across Oceanic Anoxic Event 2 of Demerara Rise, western tropical Atlantic. Geochemistry, Geophysics, Geosystems, 6(6). https://doi.org/10.1029/2004gc000850

Farouk, S., Ahmad, F., & Powell, J. H. (2017). Cenomanian–Turonian stable isotope signatures and depositional sequences in northeast Egypt and central Jordan. Journal of Asian Earth Sciences, 134, 207–230. https://doi.org/10.1016/j.jseaes.2016.11.021

Fisher, J. K., Price, G. D., Hart, M. B., & Leng, M. J. (2005). Stable isotope analysis of the Cenomanian–Turonian (Late Cretaceous) oceanic anoxic event in the Crimea. Cretaceous Research, 26(6), 853–863. https://doi.org/10.1016/j.cretres.2005.05.010

Forster, A., Kuypers, M. M. M., Turgeon, S. C., Brumsack, H.-J., Petrizzo, M. R., & Sinninghe Damsté, J. S. (2008). The Cenomanian/Turonian oceanic anoxic event in the South Atlantic: New insights from a geochemical study of DSDP Site 530A. Paleogeography,

922 Paleoclimatology, Paleoecology, 267(3–4), 256–283. https://doi.org/10.1016/j.paleo.2008.07.006

923 Forster, A., Schouten, S., Moriya, K., Wilson, P. A., & Sinninghe Damsté, J. S. (2007).
924 Tropical warming and intermittent cooling during the Cenomanian/Turonian oceanic anoxic
925 event 2: Sea surface temperature records from the equatorial Atlantic. Paleoceanography, 22(1),
926 PA1219. https://doi.org/10.1029/2006pa001349

927 Frank, M. (2002). Radiogenic isotopes: Tracers of past ocean circulation and erosional
928 input. Reviews of Geophysics, 40(1), 1–38. https://doi.org/10.1029/2000rg000094

929 Freeman, K. H., & Hayes, J. M. (1992). Fractionation of carbon isotopes by phytoplankton
930 and estimates of ancient CO_2 levels. Global Biogeochemical Cycles, 6(2), 185–198.
931 https://doi.org/10.1029/92gb00190

932 Friedrich, O., Erbacher, J., & Mutterlose, J. (2006). Paleoenvironmental changes across
933 the Cenomanian/Turonian Boundary Event (Oceanic Anoxic Event 2) as indicated by benthic
934 foraminifera from the Demerara Rise (ODP Leg 207). Revue de Micropaléontologie, 49(3), 121–
935 139. https://doi.org/10.1016/j.revmic.2006.04.003

936 Gale, A. S., & Christensen, W. K. (1996). Occurrence of the belemnite Actinocamax
937 plenus in the. Bulletin of the Geological Society of Denmark, 43(1), 68–77.

938 Gale, A. S., Jenkyns, H. C., Kennedy, W. J., & Corfield, R. M. (1993). Chemostratigraphy
939 versus biostratigraphy: data from around the Cenomanian–Turonian boundary. Journal of the
940 Geological Society, 150(1), 29–32. https://doi.org/10.1144/gsjgs.150.1.0029

941 Gale, A. S., Jenkyns, H. C., Tsikos, H., van Breugel, Y., Sinninghe Damsté, J. S., Bottini,
942 C., et al. (2019). High-resolution bio- and chemostratigraphy of an expanded record of Oceanic
943 Anoxic Event 2 (Late Cenomanian–Early Turonian) at Clot Chevalier, near Barrême, SE France

(Vocontian Basin). Newsletters on Stratigraphy, 52(1), 97–129.
https://doi.org/10.1127/nos/2018/0445

Gale, A. S., Kennedy, W. J., Voigt, S., & Walaszczyk, I. (2005). Stratigraphy of the Upper Cenomanian–Lower Turonian Chalk succession at Eastbourne, Sussex, UK: ammonites, inoceramid bivalves and stable carbon isotopes. Cretaceous Research, 26(3), 460–487.
https://doi.org/10.1016/j.cretres.2005.01.006

Gangl, S. K., Moy, C. M., Stirling, C. H., Jenkyns, H. C., Crampton, J. S., Clarkson, M. O., Ohneiser, C., & Porcelli, D. (2019). High-resolution records of Oceanic Anoxic Event 2: Insights into the timing, duration and extent of environmental perturbations from the paleo-South Pacific Ocean. Earth and Planetary Science Letters, 518, 172–182.
https://doi.org/10.1016/j.epsl.2019.04.028

Gavrilov, Y. O., Shcherbinina, E. A., Golovanova, O. V., & Pokrovskii, B. G. (2013). The late Cenomanian paleoecological event (OAE 2) in the eastern Caucasus basin of Northern Peri-Tethys. Lithology and Mineral Resources, 48(6), 457–488.
https://doi.org/10.1134/s0024490213060047

Goldstein, S. L., & Hemming, S. R. (2003). Long-lived Isotopic Tracers in Oceanography, Paleoceanography, and Ice-sheet Dynamics. Treatise on Geochemistry, 453–489.
https://doi.org/10.1016/b0-08-043751-6/06179-x

Griffiths, H. (1993). Carbon isotope discrimination. Photosynthesis and Production in a Changing Environment, 181–192. https://doi.org/10.1007/978-94-010-9626-3_11

Grosheny, D., Beaudoin, B., Morel, L., & Desmares, D. (2006). High-resolution biotratigraphy and chemostratigraphy of the Cenomanian/Turonian boundary event in the

966 Vocontian Basin, southeast France. Cretaceous Research, 27(5), 629–640.
967 https://doi.org/10.1016/j.cretres.2006.03.005

968 Grosheny, D., Ferry, S., Lécuyer, C., Thomas, A., & Desmares, D. (2017). The
969 Cenomanian–Turonian Boundary Event (CTBE) on the southern slope of the Subalpine Basin
970 (SE France) and its bearing on a probable tectonic pulse on a larger scale. Cretaceous Research,
971 72, 39–65. https://doi.org/10.1016/j.cretres.2016.11.009

972 Halliday, A. N., Davidson, J. P., Holden, P., Owen, R. M., & Olivarez, A. M. (1992).
973 Metalliferous sediments and the scavenging residence time of Nd near hydrothermal vents.
974 Geophysical Research Letters, 19(8), 761–764. https://doi.org/10.1029/92gl00393

975 Hancock, J. M. (1975). The petrology of the Chalk. Proceedings of the Geologists'
976 Association, 86(4), 499–535. https://doi.org/10.1016/s0016-7878(75)80061-7

977 Hancock, J. M. (1993). Sea-level changes around the Cenomanian–Turonian boundary.
978 Cretaceous Research, 14(4–5), 553–562. https://doi.org/10.1006/cres.1993.1039

979 Hancock, J. M., & Kauffman, E. G. (1979). The great transgressions of the Late
980 Cretaceous. Journal of the Geological Society, 136(2), 175–186.
981 https://doi.org/10.1144/gsjgs.136.2.0175

982 Hasegawa, T., Crampton, J. S., Schiøler, P., Field, B., Fukushi, K., & Kakizaki, Y. (2013).
983 Carbon isotope stratigraphy and depositional oxia through Cenomanian/Turonian boundary
984 sequences (Upper Cretaceous) in New Zealand. Cretaceous Research, 40, 61–80.
985 https://doi.org/10.1016/j.cretres.2012.05.008

986 Heimhofer, U., Wucherpfennig, N., Adatte, T., Schouten, S., Schneebeli-Hermann, E.,
987 Gardin, S., et al. (2018). Vegetation response to exceptional global warmth during Oceanic

988 Anoxic Event 2. Nature Communications, 9(1), 3832. https://doi.org/10.1038/s41467-018-
989 06319-6

990 Holmden, C., Jacobson, A. D., Sageman, B. B., & Hurtgen, M. T. (2016). Response of the
991 Cr isotope proxy to Cretaceous Ocean Anoxic Event 2 in a pelagic carbonate succession from the
992 Western Interior Seaway. Geochimica et Cosmochimica Acta, 186, 277–295.
993 https://doi.org/10.1016/j.gca.2016.04.039

994 Jarvis, I., Carson, G. A., Cooper, M. K. E., Hart, M. B., Leary, P. N., Tocher, B. A., Horne,
995 D. & Rosenfeld, A., 1988. Microfossil assemblages and the Cenomanian–Turonian (late
996 Cretaceous) oceanic anoxic event. Cretaceous Research, 9: 3–103. https://doi.org/10.1016/0195-
997 6671(88)90003-1

998 Jarvis, I., Murphy, A. M. and Gale, A. S., 2001. Geochemistry of pelagic and hemipelagic
999 carbonates: criteria for identifying systems tracts and sea-level change. Journal of the Geological
1000 Society London, 158: 685–696. https://doi.org/10.1144/jgs.158.4.685

1001 Jarvis, I., Gale, A. S., Jenkyns, H. C., & Pearce, M. A. (2006). Secular variation in Late
1002 Cretaceous carbon isotopes: a new δ13C carbonate reference curve for the Cenomanian–
1003 Campanian (99.6–70.6 Ma). Geological Magazine, 143(5), 561–608.
1004 https://doi.org/10.1017/s0016756806002421

1005 Jarvis, I., Lignum, J. S., Gröcke, D. R., Jenkyns, H. C., & Pearce, M. A. (2011). Black
1006 shale deposition, atmospheric CO_2 drawdown, and cooling during the Cenomanian–Turonian
1007 Oceanic Anoxic Event. Paleoceanography, 26(3), PA3201.
1008 https://doi.org/10.1029/2010pa002081

1009 Jeans, C. V., Long, D., Hall, M. A., Bland, D. J., & Cornford, C. (1991). The geochemistry

of the Plenus Marls at Dover, England: evidence of fluctuating oceanographic conditions and of glacial control during the development of the Cenomanian–Turonian $\delta^{13}C$ anomaly. Geological Magazine, 128(06), 603–632. https://doi.org/10.1017/s0016756800019725

Jefferies, R. P. S. (1962). The paleoecology of the Actinocamax plenus subzone (lowest Turonian) in the Anglo-Paris Basin. Paleontology, 4(4), 609–647.

Jefferies, R. P. S. (1963). The stratigraphy of the Actinocamax plenus Subzone (Turonian) in the Anglo-Paris Basin. Proceedings of the Geologists' Association, 74(1), 1–33. https://doi.org/10.1016/s0016-7878(63)80011-5

Jenkyns, H. C. (2003). Evidence for rapid climate change in the Mesozoic–Paleogene greenhouse world. Philosophical Transactions of the Royal Society of London. Series A: Mathematical, Physical and Engineering Sciences, 361(1810), 1885–1916. https://doi.org/10.1098/rsta.2003.1240

Jenkyns, H. C. (2010). Geochemistry of oceanic anoxic events. Geochemistry, Geophysics, Geosystems, 11(3), Q03004. https://doi.org/10.1029/2009gc002788

Jenkyns, H. C. (2018). Transient cooling episodes during Cretaceous Oceanic Anoxic Events with special reference to OAE 1a (Early Aptian). Philosophical Transactions of the Royal Society A: Mathematical, Physical and Engineering Sciences, 376(2130), 20170073. https://doi.org/10.1098/rsta.2017.0073

Jenkyns, H. C., Dickson, A. J., Ruhl, M., & van den Boorn, S. H. J. M. (2016). Basalt-seawater interaction, the Plenus Cold Event, enhanced weathering and geochemical change: deconstructing Oceanic Anoxic Event 2 (Cenomanian-Turonian, Late Cretaceous). Sedimentology, 64(1), 16–43. https://doi.org/10.1111/sed.12305

1032 Jenkyns, H. C., Gale, A. S., & Corfield, R. M. (1994). Carbon□ and oxygen□isotope
1033 stratigraphy of the English Chalk and Italian Scaglia and its paleoclimatic significance.
1034 Geological Magazine, 131(01), 1–34. https://doi.org/10.1017/s0016756800010451

1035 Jones, M. M., Sageman, B. B., Oakes, R. L., Parker, A. L., Leckie, R. M., Bralower, T. J.,
1036 et al. (2019). Astronomical pacing of relative sea level during Oceanic Anoxic Event 2:
1037 Preliminary studies of the expanded SH#1 Core, Utah, USA. GSA Bulletin.
1038 https://doi.org/10.1130/b32057.1

1039 Joo, Y. J., & Sageman, B. B. (2014). Cenomanian to Campanian Carbon Isotope
1040 Chemostratigraphy from the Western Interior Basin, U.S.A. Journal of Sedimentary Research,
1041 84(7), 529–542. https://doi.org/10.2110/jsr.2014.38

1042 Kaiho, K., Katabuchi, M., Oba, M., & Lamolda, M. (2014). Repeated anoxia–extinction
1043 episodes progressing from slope to shelf during the latest Cenomanian. Gondwana Research,
1044 25(4), 1357–1368. https://doi.org/10.1016/j.gr.2012.12.008

1045 Kalanat, B., Gharaie, M. H. M., Vahidinia, M., & Matsumoto, R. (2018). Short-term
1046 eustatic sea-level changes during the Cenomanian–Turonian Supergreenhouse interval in the
1047 Kopet-Dagh Basin, NE Tethyan realm. Journal of Iberian Geology, 44(2), 177–191.
1048 https://doi.org/10.1007/s41513-018-0060-8

1049 Kalanat, B., Vahidinia, M., Vaziri-Moghaddam, H., & Mahmudy-Gharaie, M. H. (2016).
1050 Planktonic foraminiferal turnover across the Cenomanian–Turonian boundary (OAE2) in the
1051 northeast of the Tethys realm, Kopet-Dagh Basin. Geologica Carpathica, 67(5), 451–462.
1052 https://doi.org/10.1515/geoca-2016-0028

1053 Kalanat, B., Vahidinia, M., Vaziri-Moghaddam, H., Mahmudy-Gharaie, M. H., & Kumon,

F. (2017). Benthic foraminiferal response to environmental changes across Cenomanian/Turonian boundary (OAE2) in the northeastern Tethys, Kopet-Dagh basin. Journal of African Earth Sciences, 134, 33–47. https://doi.org/10.1016/j.jafrearsci.2017.05.019

Keller, G., & Pardo, A. (2004). Age and paleoenvironment of the Cenomanian–Turonian global stratotype section and point at Pueblo, Colorado. Marine Micropaleontology, 51(1–2), 95–128. https://doi.org/10.1016/j.marmicro.2003.08.004

Keller, G., Adatte, T., Berner, Z., Chellai, E. H., & Stüben, D. (2008). Oceanic events and biotic effects of the Cenomanian–Turonian anoxic event, Tarfaya Basin, Morocco. Cretaceous Research, 29(5–6), 976–994. https://doi.org/10.1016/j.cretres.2008.05.020

Kelley, K. A., Plank, T., Ludden, J., & Staudigel, H. (2003). Composition of altered oceanic crust at ODP Sites 801 and 1149. Geochemistry, Geophysics, Geosystems, 4(6), 8910. https://doi.org/10.1029/2002gc000435

Kingsbury, C. G., Kamo, S. L., Ernst, R. E., Söderlund, U., & Cousens, B. L. (2018). U-Pb geochronology of the plumbing system associated with the Late Cretaceous Strand Fiord Formation, Axel Heiberg Island, Canada: part of the 130–90 Ma High Arctic large igneous province. Journal of Geodynamics, 118, 106–117. https://doi.org/10.1016/j.jog.2017.11.001

Kolonic, S., Wagner, T., Forster, A., Sinninghe Damsté, J. S., Walsworth-Bell, B., Erba, E., et al. (2005). Black shale deposition on the northwest African Shelf during the Cenomanian/Turonian oceanic anoxic event: Climate coupling and global organic carbon burial. Paleoceanography, 20(1), PA1006. https://doi.org/10.1029/2003pa000950

Košťák, M., Čech, S., Uličný, D., Sklenář, J., Ekrt, B., & Mazuch, M. (2018). Ammonites, inoceramids and stable carbon isotopes of the Cenomanian–Turonian OAE2 interval in central

Europe: Pecínov quarry, Bohemian Cretaceous Basin (Czech Republic). Cretaceous Research, 87, 150–173. https://doi.org/10.1016/j.cretres.2017.04.013

Kuhnt, W., Holbourn, A. E., Beil, S., Aquit, M., Krawczyk, T., Flögel, S., et al. (2017). Unraveling the onset of Cretaceous Oceanic Anoxic Event 2 in an extended sediment archive from the Tarfaya-Laayoune Basin, Morocco. Paleoceanography, 32(8), 923–946. https://doi.org/10.1002/2017pa003146

Kuroda, J., Ogawa, N., Tanimizu, M., Coffin, M., Tokuyama, H., Kitazato, H., & Ohkouchi, N. (2007). Contemporaneous massive subaerial volcanism and Late Cretaceous Oceanic Anoxic Event 2. Earth and Planetary Science Letters, 256(1–2), 211–223. https://doi.org/10.1016/j.epsl.2007.01.027

Kuypers, M. M. M., Pancost, R. D., & Damsté, J. S. S. (1999). A large and abrupt fall in atmospheric CO_2 concentration during Cretaceous times. Nature, 399(6734), 342–345. https://doi.org/10.1038/20659

Kuypers, M. M. M., Pancost, R. D., Nijenhuis, I. A., & Sinninghe Damsté, J. S. (2002). Enhanced productivity led to increased organic carbon burial in the euxinic North Atlantic basin during the late Cenomanian oceanic anoxic event. Paleoceanography, 17(4), 1501. https://doi.org/10.1029/2000pa000569

Lamolda, M. A., Gorostidi, A., & Paul, C. R. C. (1994). Quantitative estimates of calcareous nannofossil changes across the Plenus Marls (latest Cenomanian), Dover, England: implications for the generation of the Cenomanian–Turonian Boundary Event. Cretaceous Research, 15(2), 143–164. https://doi.org/10.1006/cres.1994.1007

Laurin, J., Barclay, R. S., Sageman, B. B., Dawson, R. R., Pagani, M., Schmitz, M., et al.

(2019). Terrestrial and marginal-marine record of the mid-Cretaceous Oceanic Anoxic Event 2 (OAE 2): High-resolution framework, carbon isotopes, CO_2 and sea-level change. Paleogeography, Paleoclimatology, Paleoecology, 524, 118–136. doi:10.1016/j.paleo.2019.03.019

Leckie, R. M. (1985). Foraminifera of the Cenomanian–Turonian Boundary Interval, Greenhorn Formation, Rock Canyon Anticline, Pueblo, Colorado. Fine-Grained Deposits and Biofacies of the Cretaceous Western Interior Seaway, 139–149. https://doi.org/10.2110/sepmfg.04.139

Li, X., Jenkyns, H. C., Wang, C., Hu, X., Chen, X., Wei, Y., et al. (2006). Upper Cretaceous carbon- and oxygen-isotope stratigraphy of hemipelagic carbonate facies from southern Tibet, China. Journal of the Geological Society, 163(2), 375–382. https://doi.org/10.1144/0016-764905-046

Lu, Z., Jenkyns, H. C., & Rickaby, R. E. M. (2010). Iodine to calcium ratios in marine carbonate as a paleo-redox proxy during oceanic anoxic events. Geology, 38(12), 1107–1110. https://doi.org/10.1130/g31145.1

MacLeod, K. G., Martin, E. E., & Blair, S. W. (2008). Nd isotopic excursion across Cretaceous ocean anoxic event 2 (Cenomanian–Turonian) in the tropical North Atlantic. Geology, 36(10), 811–814. https://doi.org/10.1130/g24999a.1

Maher, Jr., H. D. (2001). Manifestations of the Cretaceous High Arctic Large Igneous Province in Svalbard. The Journal of Geology, 109(1), 91–104. https://doi.org/10.1086/317960

Martin, E. E., MacLeod, K. G., Jiménez Berrocoso, A., & Bourbon, E. (2012). Water mass circulation on Demerara Rise during the Late Cretaceous based on Nd isotopes. Earth and

1120 Planetary Science Letters, 327–328, 111–120. https://doi.org/10.1016/j.epsl.2012.01.037

1121 Monteiro, F. M., Pancost, R. D., Ridgwell, A., & Donnadieu, Y. (2012). Nutrients as the
1122 dominant control on the spread of anoxia and euxinia across the Cenomanian–Turonian oceanic
1123 anoxic event (OAE2): Model–data comparison. Paleoceanography, 27(4), PA4209.
1124 https://doi.org/10.1029/2012pa002351

1125 Mort, H., Jacquat, O., Adatte, T., Steinmann, P., Föllmi, K., Matera, V., et al. (2007). The
1126 Cenomanian/Turonian anoxic event at the Bonarelli Level in Italy and Spain: enhanced
1127 productivity and/or better preservation? Cretaceous Research, 28(4), 597–612.
1128 https://doi.org/10.1016/j.cretres.2006.09.003

1129 Navarro-Ramirez, J. P., Bodin, S., & Immenhauser, A. (2016). Ongoing Cenomanian–
1130 Turonian heterozoan carbonate production in the neritic settings of Peru. Sedimentary Geology,
1131 331, 78–93. https://doi.org/10.1016/j.sedgeo.2015.10.011

1132 Navarro-Ramirez, J. P., Bodin, S., Consorti, L., & Immenhauser, A. (2017). Response of
1133 western South American epeiric-neritic ecosystem to middle Cretaceous Oceanic Anoxic Events.
1134 Cretaceous Research, 75, 61–80. https://doi.org/10.1016/j.cretres.2017.03.009

1135 Nederbragt, A. J., & Fiorentino, A. (1999). Stratigraphy and paleoceanography of the
1136 Cenomanian–Turonian Boundary Event in Oued Mellegue, north-western Tunisia. Cretaceous
1137 Research, 20(1), 47–62. https://doi.org/10.1006/cres.1998.0136

1138 Nemoto, T., & Hasegawa, T. (2011). Submillennial resolution carbon isotope stratigraphy
1139 across the Oceanic Anoxic Event 2 horizon in the Tappu section, Hokkaido, Japan.
1140 Paleogeography, Paleoclimatology, Paleoecology, 309(3–4), 271–280.
1141 https://doi.org/10.1016/j.paleo.2011.06.009

O'Brien, C.L., Robinson, S.A., Pancost, R.D., Sinninghe Damsté, J.S., Schouten, S., Lunt, D.J., Alsenz, H., Bornemann, A., Bottini, C., Brassell, S.C., Farnsworth, A., Forster, A., Huber, B.T., Inglis, G.N., Jenkyns, H.C., Linnert, C., Littler, K., Markwick, P., McAnena, A., Mutterlose, J., Naafs, B.D.A., Püttmann, W., Sluijs, A., van Helmond, A.G.M., Vellekoop, J., Wagner, T. & Wrobel., N.E. 2017., Cretaceous sea-surface temperature evolution: Constraints from TEX_{86} and planktonic foraminiferal oxygen isotopes. Earth-Science Reviews 172, 224–247.

Orth, C. J., Attrep, M., Quintana, L. R., Elder, W. P., Kauffman, E. G., Diner, R., & Villamil, T. (1993). Elemental abundance anomalies in the late Cenomanian extinction interval: a search for the source(s). Earth and Planetary Science Letters, 117(1–2), 189–204. https://doi.org/10.1016/0012-821x(93)90126-t

Ostrander, C. M., Owens, J. D., & Nielsen, S. G. (2017). Constraining the rate of oceanic deoxygenation leading up to a Cretaceous Oceanic Anoxic Event (OAE-2: ~94 Ma). Science Advances, 3(8), e1701020. https://doi.org/10.1126/sciadv.1701020

Owens, J. D., Gill, B. C., Jenkyns, H. C., Bates, S. M., Severmann, S., Kuypers, M. M. M., et al. (2013). Sulfur isotopes track the global extent and dynamics of euxinia during Cretaceous Oceanic Anoxic Event 2. Proceedings of the National Academy of Sciences, 110(46), 18407–18412. https://doi.org/10.1073/pnas.1305304110

Parente, M., Frijia, G., Di Lucia, M., Jenkyns, H. C., Woodfine, R. G., & Baroncini, F. (2008). Stepwise extinction of larger foraminifers at the Cenomanian–Turonian boundary: A shallow-water perspective on nutrient fluctuations during Oceanic Anoxic Event 2 (Bonarelli Event). Geology, 36(9), 715–718. https://doi.org/10.1130/g24893a.1

1164 Paul, C. R. C., Lamolda, M. A., Mitchell, S. F., Vaziri, M. R., Gorostidi, A., & Marshall, J.
1165 D. (1999). The Cenomanian–Turonian boundary at Eastbourne (Sussex, UK): a proposed
1166 European reference section. Paleogeography, Paleoclimatology, Paleoecology, 150(1–2), 83-121.
1167 https://doi.org/10.1016/s0031-0182(99)00009-7

1168 Pearce, M. A., Jarvis, I., & Tocher, B. A. (2009). The Cenomanian–Turonian boundary
1169 event, OAE2 and paleoenvironmental change in epicontinental seas: New insights from the
1170 dinocyst and geochemical records. Paleogeography, Paleoclimatology, Paleoecology, 280(1–2),
1171 207–234. https://doi.org/10.1016/j.paleo.2009.06.012

1172 Pedersen, T.F. & Calvert, S.E. (1990). Anoxia vs. Productivity: What Controls the
1173 Formation of Organic-Carbon-Rich Sediments and Sedimentary Rocks? AAPG Bulletin, 74(4),
1174 454–466. https://doi.org/10.1306/0c9b232b-1710-11d7-8645000102c1865d

1175 Peryt, D., & Lamolda, M. (1996). Benthonic foraminiferal mass extinction and survival
1176 assemblages from the Cenomanian–Turonian Boundary Event in the Menoyo Section, northern
1177 Spain. Geological Society, London, Special Publications, 102(1), 245–258.
1178 https://doi.org/10.1144/gsl.sp.1996.001.01.18

1179 Pogge von Strandmann, P. A. E., Jenkyns, H. C., & Woodfine, R. G. (2013). Lithium
1180 isotope evidence for enhanced weathering during Oceanic Anoxic Event 2. Nature Geoscience,
1181 6(8), 668–672. https://doi.org/10.1038/ngeo1875

1182 Pratt, L.M., 1985, Isotopic studies of organic matter and carbonate in rocks of the
1183 Greenhorn Marine Cycle, *In* Pratt, L.M., et al., eds., Fine-grained deposits and biofacies of the
1184 Cretaceous Western Interior Seaway: Evidence of cyclic sedimentary processes: SEPM Field
1185 Trip Guidebook No. 4, 38–48. https://doi.org/10.2110/sepmfg.04

1186 Prokoph, A., Babalola, L. O., El Bilali, H., Olagoke, S., & Rachold, V. (2013).
1187 Cenomanian–Turonian carbon isotope stratigraphy of the Western Canadian Sedimentary Basin.
1188 Cretaceous Research, 44, 39–53. https://doi.org/10.1016/j.cretres.2013.03.005

1189 Robinson, S. A., Dickson, A. J., Pain, A., Jenkyns, H. C., O'Brien, C. L., Farnsworth, A., &
1190 Lunt, D. J. (2019). Southern Hemisphere sea-surface temperatures during the Cenomanian–
1191 Turonian: Implications for the termination of Anoxic Event 2. Geology, 47(2), 131–134.
1192 https://doi.org/10.1130/g45842.1

1193 Rudnick, R. L., & Gao, S. (2014). Composition of the continental crust. *Treatise on*
1194 *geochemistry*, *3*, 659. https://doi.org/10.1016/b978-0-08-095975-7.00301-6

1195 Sageman, B. B., Meyers, S. R., & Arthur, M. A. (2006). Orbital time scale and new C-
1196 isotope record for Cenomanian–Turonian boundary stratotype. Geology, 34(2), 125.
1197 https://doi.org/10.1130/g22074.1

1198 Scaife, J. D., Ruhl, M., Dickson, A. J., Mather, T. A., Jenkyns, H. C., Percival, L. M. E., et
1199 al. (2017). Sedimentary Mercury Enrichments as a Marker for Submarine Large Igneous
1200 Province Volcanism? Evidence from the Mid-Cenomanian Event and Oceanic Anoxic Event 2
1201 (Late Cretaceous). Geochemistry, Geophysics, Geosystems, 18(12), 4253–4275.
1202 https://doi.org/10.1002/2017gc007153

1203 Schlanger, S. O., & Jenkyns, H. C. (1976). Cretaceous oceanic anoxic events: causes and
1204 consequences. Geologie en mijnbouw, 55(3–4).

1205 Schlanger, S. O., Arthur, M. A., Jenkyns, H. C., & Scholle, P. A. (1987). The
1206 Cenomanian–Turonian Oceanic Anoxic Event, I. Stratigraphy and distribution of organic carbon-
1207 rich beds and the marine $\delta^{13}C$ excursion. Geological Society, London, Special Publications,

26(1), 371–399. https://doi.org/10.1144/gsl.sp.1987.026.01.24

Scholle, P. A. (1974). Diagenesis of Upper Cretaceous chalks from England, Northern Ireland and the North Sea. *In* Hsü, K. J., & Jenkyns, H. C. (Eds.). *Pelagic Sediments: On Land and Under the Sea* (Vol. 70). John Wiley & Sons. https://doi.org/10.1002/9781444304855.ch8

Scholle, P.A., & Arthur, M.A. (1980). Carbon Isotope Fluctuations in Cretaceous Pelagic Limestones: Potential Stratigraphic and Petroleum Exploration Tool. AAPG Bulletin, 60(1), 67–87. https://doi.org/10.1306/2f91892d-16ce-11d7-8645000102c1865d

Schröder-Adams, C. J., Herrle, J. O., Selby, D., Quesnel, A., & Froude, G. (2019). Influence of the High Arctic Igneous Province on the Cenomanian/Turonian boundary interval, Sverdrup Basin, High Canadian Arctic. Earth and Planetary Science Letters, 511, 76–88. https://doi.org/10.1016/j.epsl.2019.01.023

Sinninghe Damsté, J. S., van Bentum, E. C., Reichart, G.□J., Pross, J., & Schouten, S. (2010). A CO_2 decrease□driven cooling and increased latitudinal temperature gradient during the mid□Cretaceous Oceanic Anoxic Event 2. *Earth and Planetary Science Letters*, *293*(1–2), 97–103. https://doi.org/10.1016/j.epsl.2010.02.027

Snow, L. J., Duncan, R. A., & Bralower, T. J. (2005). Trace element abundances in the Rock Canyon Anticline, Pueblo, Colorado, marine sedimentary section and their relationship to Caribbean plateau construction and oxygen anoxic event 2. Paleoceanography, 20(3), PA3005. https://doi.org/10.1029/2004pa001093

Sweere, T. C., Dickson, A. J., Jenkyns, H. C., Porcelli, D., Elrick, M., van den Boorn, S. H. J. M., & Henderson, G. M. (2018). Isotopic evidence for changes in the zinc cycle during Oceanic Anoxic Event 2 (Late Cretaceous). Geology, 46(5), 463–466.

https://doi.org/10.1130/g40226.1

Takashima, R., Nishi, H., Hayashi, K., Okada, H., Kawahata, H., Yamanaka, T., et al. (2009). Litho-, bio- and chemostratigraphy across the Cenomanian/Turonian boundary (OAE 2) in the Vocontian Basin of southeastern France. Paleogeography, Paleoclimatology, Paleoecology, 273(1–2), 61–74. https://doi.org/10.1016/j.paleo.2008.12.001

Takashima, R., Nishi, H., Hayashi, K., Okada, H., Kawahata, H., Yamanaka, T., et al. (2009). Litho-, bio- and chemostratigraphy across the Cenomanian/Turonian boundary (OAE 2) in the Vocontian Basin of southeastern France. Paleogeography, Paleoclimatology, Paleoecology, 273(1–2), 61–74. https://doi.org/10.1016/j.paleo.2008.12.001

Tanaka, T., Togashi, S., Kamioka, H., Amakawa, H., Kagami, H., Hamamoto, T., et al. (2000). JNdi-1: a neodymium isotopic reference in consistency with LaJolla neodymium. Chemical Geology, 168(3–4), 279–281. https://doi.org/10.1016/s0009-2541(00)00198-4

Taylor, S. R., & McLennan, S. M. (1995). The geochemical evolution of the continental crust. Reviews of Geophysics, 33(2), 241. https://doi.org/10.1029/95rg00262

Tegner, C., Storey, M., Holm, P. M., Thorarinsson, S. B., Zhao, X., Lo, C.-H., & Knudsen, M. F. (2011). Magmatism and Eurekan deformation in the High Arctic Large Igneous Province: ^{40}Ar–^{39}Ar age of Kap Washington Group volcanics, North Greenland. Earth and Planetary Science Letters, 303(3-4), 203–214. https://doi.org/10.1016/j.epsl.2010.12.047

Thomas, D. J., & Tilghman, D. S. (2014). Geographically different oceanographic responses to global warming during the Cenomanian–Turonian interval and Oceanic Anoxic Event 2. Paleogeography, Paleoclimatology, Paleoecology, 411, 136–143. https://doi.org/10.1016/j.paleo.2014.06.014

Tostevin, R., Shields, G. A., Tarbuck, G. M., He, T., Clarkson, M. O., & Wood, R. A. (2016). Effective use of cerium anomalies as a redox proxy in carbonate-dominated marine settings. Chemical Geology, 438, 146–162. https://doi.org/10.1016/j.chemgeo.2016.06.027

Trabucho-Alexandre, J. (2014). More gaps than shale: erosion of mud and its effect on preserved geochemical and paleobiological signals. Geological Society, London, Special Publications, 404(1), 251–270. https://doi.org/10.1144/sp404.10

Tsikos, H., Jenkyns, H. C., Walsworth-Bell, B., Petrizzo, M. R., Forster, A., Kolonic, S., et al. (2004). Carbon-isotope stratigraphy recorded by the Cenomanian–Turonian Oceanic Anoxic Event: correlation and implications based on three key localities. Journal of the Geological Society, 161(4), 711–719. https://doi.org/10.1144/0016-764903-077

Turgeon, S. C., & Creaser, R. A. (2008). Cretaceous oceanic anoxic event 2 triggered by a massive magmatic episode. Nature, 454(7202), 323–326. https://doi.org/10.1038/nature07076

Van Bentum, E. C., Reichart, G.-J., Forster, A., & Sinninghe Damsté, J. S. (2012). Latitudinal differences in the amplitude of the OAE-2 carbon isotopic excursion: CO_2 and paleo productivity. Biogeosciences, 9(2), 717–731. https://doi.org/10.5194/bg-9-717-2012

van Helmond, N. A. G. M., Ruvalcaba Baroni, I., Sluijs, A., Sinninghe Damsté, J. S., & Slomp, C. P. (2014). Spatial extent and degree of oxygen depletion in the deep proto□North Atlantic basin during Oceanic Anoxic Event 2. Geochemistry, Geophysics, Geosystems, 15, 4254–4266. https://doi.org/10.1002/2014GC005528

Van Helmond, N. A. G. M., Sluijs, A., Papadomanolaki, N. M., Plint, A. G., Gröcke, D. R., Pearce, M. A., et al. (2016). Equatorward phytoplankton migration during a cold spell within the Late Cretaceous super-greenhouse. Biogeosciences, 13(9), 2859–2872.

https://doi.org/10.5194/bg-13-2859-2016

Van Helmond, N. A. G. M., Sluijs, A., Reichart, G.-J., Sinninghe Damsté, J. S., Slomp, C. P., & Brinkhuis, H. (2013). A perturbed hydrological cycle during Oceanic Anoxic Event 2. Geology, 42(2), 123–126. https://doi.org/10.1130/g34929.1

van Helmond, N. A. G. M., Sluijs, A., Sinninghe Damsté, J. S., Reichart, G.□J., Voigt, S., Erbacher, J., et al. (2015). Freshwater discharge controlled deposition of Cenomanian–Turonian black shales on the NW European epicontinental shelf (Wunstorf, northern Germany). Climate of the Past, 11(3), 495–508. https://doi.org/10.5194/cp□11□495□2015

van Hinsbergen, D. J. J., de Groot, L. V., van Schaik, S. J., Spakman, W., Bijl, P. K., Sluijs, A., et al. (2015). A paleolatitude calculator for paleoclimate studies. PLoS ONE, 10(6), e0126946. https://doi.org/10.1371/journal.pone.0126946

Voigt, S. (2000). Cenomanian–Turonian composite $\delta^{13}C$ curve for Western and Central Europe: the role of organic and inorganic carbon fluxes. Paleogeography, Paleoclimatology, Paleoecology, 160(1–2), 91–104. https://doi.org/10.1016/s0031-0182(00)00060-2

Voigt, S., Aurag, A., Leis, F., & Kaplan, U. (2007). Late Cenomanian to Middle Turonian high-resolution carbon isotope stratigraphy: New data from the Münsterland Cretaceous Basin, Germany. Earth and Planetary Science Letters, 253(1-2), 196–210. https://doi.org/10.1016/j.epsl.2006.10.026

Voigt, S., Erbacher, J., Mutterlose, J., Weiss, W., Westerhold, T., Wiese, F., et al. (2008). The Cenomanian–Turonian of the Wunstorf section – (North Germany): global stratigraphic reference section and new orbital time scale for Oceanic Anoxic Event 2. Newsletters on Stratigraphy, 43(1), 65–89. https://doi.org/10.1127/0078-0421/2008/0043-0065

1296 Voigt, S., Gale, A. S., & Flögel, S. (2004). Midlatitude shelf seas in the Cenomanian–
1297 Turonian greenhouse world: Temperature evolution and North Atlantic circulation.
1298 Paleoceanography, 19, PA4020. https://doi.org/10.1029/2004PA001015

1299 Voigt, S., Gale, A. S., & Voigt, T. (2006). Sea-level change, carbon cycling and
1300 paleoclimate during the Late Cenomanian of northwest Europe; an integrated
1301 paleoenvironmental analysis. Cretaceous Research, 27(6), 836–858.
1302 https://doi.org/10.1016/j.cretres.2006.04.005

1303 Webb, G. E., & Kamber, B. S. (2000). Rare earth elements in Holocene reefal
1304 microbialites: a new shallow seawater proxy. Geochimica et Cosmochimica Acta, 64(9), 1557–
1305 1565. https://doi.org/10.1016/S0016-7037(99)00400-7

1306 Wendler, I. (2013). A critical evaluation of carbon isotope stratigraphy and biostratigraphic
1307 implications for Late Cretaceous global correlation. Earth-Science Reviews, 126, 116–146.
1308 https://doi.org/10.1016/j.earscirev.2013.08.003

1309 Wendler, J. E., Wendler, I., Vogt, C., & Kuss, J. (2016). Link between cyclic eustatic sea-
1310 level change and continental weathering: Evidence for aquifer-eustasy in the Cretaceous.
1311 Paleogeography, Paleoclimatology, Paleoecology, 441, 430–437.
1312 https://doi.org/10.1016/j.paleo.2015.08.014

1313 Zaghbib-Turki, D., & Soua, M. (2013). High resolution biostratigraphy of the
1314 Cenomanian–Turonian interval (OAE2) based on planktonic foraminiferal bioevents in North-
1315 Central Tunisia. Journal of African Earth Sciences, 78, 97–108.
1316 https://doi.org/10.1016/j.jafrearsci.2012.09.014

1317 Zheng, X.-Y., Jenkyns, H. C., Gale, A. S., Ward, D. J., & Henderson, G. M. (2013).

Changing ocean circulation and hydrothermal inputs during Ocean Anoxic Event 2 (Cenomanian–Turonian): Evidence from Nd-isotopes in the European shelf sea. Earth and Planetary Science Letters, 375, 338–348. https://doi.org/10.1016/j.epsl.2013.05.053

Zheng, X.-Y., Jenkyns, H. C., Gale, A. S., Ward, D. J., & Henderson, G. M. (2016). A climatic control on reorganization of ocean circulation during the mid-Cenomanian event and Cenomanian–Turonian oceanic anoxic event (OAE 2): Nd isotope evidence. Geology, 44(2), 151–154. https://doi.org/10.1130/g37354.1

Zhou, X., Jenkyns, H. C., Owens, J. D., Junium, C. K., Zheng, X.-Y., Sageman, B. B., et al. (2015). Upper ocean oxygenation dynamics from I/Ca ratios during the Cenomanian-Turonian OAE 2. Paleoceanography, 30(5), 510–526. https://doi.org/10.1002/2014pa002741

Figure 1. The composite 'type-section' recording OAE 2 and the Plenus Cold Event from the English Chalk, using $\delta^{13}C_{carb}$ from Eastbourne (Tsikos et al., 2004), and bulk $\delta^{18}O$ and boreal fauna from Dover (Lamolda et al., 1994; Gale and Christensen, 1996), correlated using the beds of the Plenus Marl Member (for details see Jarvis et al., 2006). Points 'a–d' show globally consistent positions on the $\delta^{13}C$ curve (Jarvis et al., 2006). The gray box shows the interval of OAE 2 (Jenkyns et al., 2017) extending from the uppermost Cenomanian to the lowermost Turonian. The red bar indicates the Plenus carbon-isotope excursion, as defined in this study. The blue bars indicate cooling, with the upper bar defined in this study as the PCE *sensu stricto* (Gale and Christensen, 1996).

Figure 2. New geochemical data from the Plenus Marls at Dover, UK. Points 'a' and 'b' are identified on the $\delta^{13}C$ curve. With the exception of ε_{Nd}, error bars are smaller than the data points. The red dotted line indicates the onset of OAE 2; the red bar indicates the Plenus carbon-isotope excursion; the blue bar indicates the PCE *sensu stricto*.

Figure 3. Global distribution of known records demonstrating the Plenus CIE (a negative $\delta^{13}C$ excursion between points 'a' and 'b' in Figure 1) or an excursion in CO_2 across the Plenus interval, as indicated by $\Delta^{13}C$, compound-specific $\delta^{13}C$, or leaf stomata. **1** Pratt's Landing (van Helmond et al., 2016); Vermillion River, Well 10-35-45-2WA (Prokoph et al., 2013). **2** Cuba, KS (Bowman & Bralower 2015); Pueblo (Barclay et al., 2010; Bowman & Bralower, 2005; Caron et al., 2006; Keller et al., 2008; Pratt et al., 1985; Sageman et al., 2006); USGS Portland-1 core (Eldrett et al., 2017); Aristocrat Angus core (Joo and Sageman, 2014); Hot Springs, CO (Desmares et al., 2007); SH#1 core (Jones et al., 2019); generalized Western Interior Seaway

(Orth et al., 1993). **3** Great Valley Sequence, CA (Du Vivier et al., 2015). **4** Innes-1 core, Iona-1 core, Well X core (Eldrett et al., 2017). **5** Axaxacoalco, Barranca el Tigre, Barranco el Canon (Elrick et al., 2009). **6** Laurichocha, Piedra Parada, Uchucchacua (Navarro-Ramirez et al., 2016, 2017). **7** Bass River, NJ (Bowman and Bralower, 2005; van Helmond et al., 2013). **8** ODP Site 1258 (Erbacher et al., 2005); ODP Site 1260 (Eldrett et al., 2017; Erbacher et al., 2005; Forster et al., 2007: van Bentum et al., 2012); ODP Site 1261 (Eldrett et al., 2017; Erbacher et al., 2005). **9** DSDP Site 367 (Dickson et al., 2016; Forster et al., 2007; Kuypers et al., 1999; Sinninghe Damsté et al., 2008). **10** Tarfaya (Keller et al., 2008; Kolonic et al., 2005; Kuhnt et al., 2017; Kuypers et al., 2002; Tsikos et al., 2004); Mpl, S57, S75 (Kolonic et al., 2005); S13 (Kuypers et al., 1999; Kolonic et al., 2005). **11** ODP Site 1276 (Sinninghe Damsté et al., 2008; van Helmond et al., 2014). **12** Arobes, Ganuza, Menoyo (Kaiho et al., 2014); Manilvala (Mort et al., 2007); Puentedey (Barroso-Barcenilla et al., 2011). **13** Dover (this study; Jeans et al., 1991; Lamolda et al., 1994); Eastbourne (Jenkyns et al., 1994; Paul et al., 1999; Tsikos et al., 2004; Gale et al., 2005; Pearce et al., 2009; Zheng et al., 2013); Culver Cliff (Jarvis et al., 2001). **14** Gröbern (Voigt et al., 2006); Halle (Voigt et al., 2007); Wunstorf (Voigt et al., 2008; Du Vivier et al., 2014); Roter Sattel (Charbonnier et al., 2018). **15** Lambruisse (Takashima et al., 2009); Pont d'Issole (Grosheny et al., 2006; Jarvis et al., 2011); les Lattes, Le Bourgeut (Grosheny et al., 2017); Cassis (Heimhofer et al., 2018); Clot Chevalier (Gale et al., 2019). **16** Pecínov, Czech Republic (Košťák et al., 2017). **17** Bottaccione (Kuroda et al., 2007); Furlo (Mort et al., 2007); Gubbio (Jenkyns et al., 1994; Tsikos et al., 2004); Raia del Pedale (Owens et al., 2013); Monte Coccovello, Monte Varchera (Parente et al., 2008). **18** Crimea (Fisher et al., 2005). **19** Jerissa (Zaghbib-Turki & Soua 2013); Oued Mellegue (Nederbragt & Fiorentino 1999); Wadi Bahoul (Caron et al., 2006). **20** Wadi Feiran (El-Sabbagh et al., 2011). **21** Ghawr Al Mazar (Wendler et

al., 2016); Wadi Karak (Farouk et al., 2017). **22** Aimaki, Khadzhalmakhi, Levashi (Gavrilov et al., 2013). **23** Taherabad (Kalanat et al., 2018). **24** Tappu (Nemoto & Hasegawa 2011); Yezo (Du Vivier et al., 2015). **25** ODP Site 530 (Forster et al., 2008). **26** Gongzha (Bomou et al., 2013); Tingri (Li et al., 2006). **27** Sawpit Gully, Mangaotane B (Hasegawa et al., 2013; Gangl et al., 2019); Mangaotane A (Hasegawa et al., 2013).

Figure 4. Comparison of $\delta^{13}C_{org}$ and $\delta^{13}C_{hopane}$ records from ODP Site 1276, Cape Verde Basin (adapted from Sinninghe Damsté et al., 2010) demonstrating a stratigraphic offset in the position of the negative excursion seen in $\delta^{13}C_{org}$ at ~1083.1 mbsf and in $\delta^{13}C_{hopane}$ at ~1082.8 mbsf.

Figure 5. Records of CO_2 change across the Plenus interval. The gray boxes indicate the OAE 2 interval; the red boxes indicate the P-CIE; the blue boxes indicate the PCE *sensu stricto*; points 'a' to 'c' of the OAE are labelled. Coloured bands illustrate visual approximations of trends.

Figure 6. Global distribution of known records demonstrating a change in temperature across the PCE interval, based on records of TEX_{86}, $\delta^{18}O$, faunal assemblages, and foraminiferal coiling. **1** Pratt's Landing (van Helmond et al., 2016). **2** Hot Springs, SD (Desmares et al., 2016); Pueblo (Caron et al., 2006; Desmares et al., 2016); USGS Portland-1 Core (Eldrett et al., 2017). **3** Iona-1 core, Innes-1 core, Well X core (Eldrett et al., 2017). **4** Bass River, NJ (van Helmond et al., 2013). **5** ODP Site 1260 (Forster et al., 2007; Eldrett et al., 2017). **6** DSDP Site 367 (Forster et al., 2007). **7** Tarfaya (Tsikos et al., 2004; Kuhnt et al., 2017). **8** ODP Site 1276 (Sinninghe Damsté et al., 2008). **9** Arobes, Ganuza, Menoyo (Kaiho et al., 2014); Puentedey (Barroso-

Barcenilla et al., 2011). **10** Dover (this study; Jefferies 1962; Jeans et al., 1991; Lamolda et al., 1994); Eastbourne (Jenkyns et al., 1994; Paul et al., 1999; Tsikos et al., 2004; Voigt et al., 2004, 2006; Pearce et al., 2009; Zheng et al., 2013). **11** Gröbern (Voigt et al., 2006); Halle (Voigt et al., 2007); Wunstorf (van Helmond et al., 2015). **12** Cassis (Heimhofer et al., 2018); Clot Chevalier (Gale et al., 2019); Lambruisse (Takashima et al., 2009); les Lettes (Gale & Christensen 1996); Pont d'Issole (Jarvis et al., 2011). **13** Gubbio (Jenkyns et al., 1994). **14** Crimea (Fisher et al., 2005). **15** Oued Mellegue (Nederbragt & Fiorentino 1999); Wadi Bahoul (Caron et al., 2006). **16** Wadi Karak (Farouk et al., 2017). **17** Amaki, Khadzhalmakhi, Levashi (Gavrilov et al., 2013). **18** Taherabad (Kalanat et al., 2018).

Figure 7. Records of SSTs during the Plenus interval. The gray boxes indicate the OAE 2 interval; the red boxes indicate the P-CIE; the blue boxes indicate the PCE *sensu stricto*; points 'a' to 'c' of the OAE are labelled. Dover stratigraphy from Lamolda et al., 1994; Wunstorf stratigraphy from Voigt et al., 2008. Coloured bands illustrate visual approximations of trends.

Figure 8. Global distribution of known records demonstrating a change in water-mass character across the Plenus interval, as indicated by elemental, isotopic, lithological, or faunal changes in the sedimentary record. **1** Vermillion River (Prokoph et al., 2013). **2** Angus Aristocrat core (Zhou et al., 2015); Cuba, KS (Bowman & Bralower 2015; Elderbak et al., 2014); Hot Springs, SD (Desmares et al., 2016); USGS Portland-1 core (Du Vivier et al., 2014; Holmden et al., 2016; Eldrett et al., 2017); generalized Western Interior Seaway (Orth et al., 1993); Pueblo (Bowman & Bralower, 2005; Caron et al., 2006; Keller et al., 2008; Elderbak et al., 2014). **3** Great Valley Sequence, CA (Du Vivier et al., 2015). **4** Innes-1 core, Iona-1 core, Well X core (Eldrett et al.,

2017). **5** Barranco el Canon (Elrick et al., 2009; Sweere et al., 2018). **6** Bass River, NJ (Bowman and Bralower, 2005). **7** ODP Site 1258 (Erbacher et al., 2005; Friedrich et al., 2006; Ostrander et al., 2017; Zhou et al., 2015); ODP Site 1260 (Erbacher et al., 2005; Friedrich et al., 2006; Forster et al., 2007; Turgeon and Creaser, 2008; Du Vivier et al., 2014; Eldrett et al., 2017); ODP Site 1261 (Erbacher et al., 2005; Friedrich et al., 2006). **8** DSDP Site 367 (Kuypers et al., 1999; Forster et al., 2007, 2008; Sinninghe Damsté et al., 2008; Du Vivier et al., 2014; Dickson et al., 2016). **9** Tarfaya (Kuypers et al., 2002; Tsikos et al., 2004; Keller et al., 2008; Dickson et al., 2016; Kuhnt et al., 2017); Mpl, S13, S57, S75 (Kolonic et al., 2005). **10** ODP Site 1276 (Sinninghe Damsté et al., 2008; van Helmond et al., 2014). **11** Puentedey (Barroso-Barcenilla et al., 2011); Arobes (Kaiho et al., 2014); Ganuza (Peryt and Lamolda, 1995; Kaiho et al., 2014); Manivala (Mort et al., 2007); Menoyo (Peryt and Lamolda, 1995; Kaiho et al., 2014). **12** Dover (this study; Jeans et al., 1991); Eastbourne (Orth et al., 1993; Paul et al., 1999; Pearce et al., 2009; Lu et al., 2010; Owens et al., 2013; Zheng et al., 2013; Zhou et al., 2015; Clarkson et al., 2018; Sweere et al., 2018). **13** Wunstorf (van Helmond et al., 2015); Halle (Voigt et al., 2007); Roter Sattel (Charbonnier et al., 2018); Wunstorf (Du Vivier et al., 2014; van Helmond et al., 2015). **14** Clot Chevalier (Gale et al., 2019); Lambruisse (Takashima et al., 2009); Le Bourgeut (Grosheny et al., 2017); Pont d'Issole (Grosheny et al., 2006; Jarvis et al., 2011; Danzelle et al., 2018); Vocontian Basin (Du Vivier et al., 2014). **15** Bottaccione (Kuroda et al., 2007); Furlo (Mort et al., 2007); Gubbio (Tsikos et al., 2004); Raia del Pedale (Owens et al., 2013; Zhou et al., 2015; Clarkson et al., 2018; Sweere et al., 2018). **16** Crimea (Fisher et al., 2005). **17** Oued Mellegue (Nederbragt & Fiorentino 1999); Wadi Bahoul (Caron et al., 2006). **18** Wadi Feiran (El-Sabbagh et al., 2011). **19** Wadi Karak (Farouk et al., 2018). **20** Aimaki, Khadzhalmakhi, Levashi (Gavrilov et al., 2013). **21** Gharesu (Kalanat et al., 2016); Taherabad (Kalanat et al.,

2016, 2017). **22** Tappu (Nemoto & Hasegawa 2011); Yezo Group (Du Vivier et al., 2015). **23** DSDP Site 530 (Forster et al., 2008; Du Vivier et al., 2014). **24** Gongzha (Bomou et al., 2013).

Figure 9. Potential models for cooling during the PCE. $\delta^{13}C$ from Eastbourne (Tsikos et al., 2004). The gray box indicates the OAE 2 interval; the red box indicates the P-CIE; points 'a' to 'd' of the $\delta^{13}C$ curve are labelled. The red lines indicate CO_2, the blue lines indicate SST, and the green line indicates circulation. Values are arbitrary. Model (1): a direct link between CO_2, atmospheric temperatures, and SSTs would produce a cooling interval after a drop in CO_2. Model (2): a fall in CO_2 would drive global temperature decrease, forcing a circulation change and, in turn, further cooling. In this model, cooling must come after the CO_2 change. Model (3): no direct link between CO_2 and SSTs would produce variable timing and expression of temperatures at individual sites.